Acceleration hotspots of North American birds' decline are associated with agriculture

François Leroy [1,2], Marta A. Jarzyna [2,3], Petr Keil [1]*

[1]Department of Spatial Sciences, Faculty of Environmental Sciences, Czech University of Life Sciences Prague, Kamýcká 129, 16500 Praha-Suchdol, Czech Republic

[2] Department of Evolution, Ecology and Organismal Biology, The Ohio State University, Columbus, Ohio, 43210, USA

[3] Translational Data Analytics Institute, The Ohio State University, Columbus, Ohio, 43210, USA

Abstract

Human activities might have accelerated declines of population abundance, but this acceleration remains underexplored. Using 1033 North American Breeding Bird Survey routes, we analyze abundance change and its acceleration for 261 bird species, 54 avian families, and 10 habitats from 1987 to 2021. We show an average continent-wide decline of abundance of all birds per local route, with hotspots of decline in southern and warm parts of North America, and hotspots of accelerating decline in the Mid-Atlantic, Midwest, and California, matching patterns of agricultural intensity. Overall, 122 species (47%) exhibit significant declines, of which 63 also show acceleration of this decline, and 67 show declining per-capita growth rate, raising concerns for a large part of North American bird populations. These findings suggest that bird abundance decline is mostly accelerating, with spatial patterns of this acceleration indicating that agricultural intensity may be a driver of this trend.

Main text

Human activities such as land-use change, agricultural intensification, overexploitation, and pollution have significantly impacted ecosystems over the past centuries [IPBES (*1*)]. Temporal changes in local population abundances are closely monitored indicators of this impact (*2*), and have shown an overall abundance decline across taxa (*1*, *3*). The past century, however, has seen not only the increase but also an acceleration in the increase of human activities, sometimes termed the Great Acceleration (*4–6*), and a likely acceleration of global vertebrate extinction rates (*7–9*). We should thus expect a corresponding acceleration in population declines. In essence, while the first-order derivative of population abundance over time for many species appears to be a decline, the second-order derivative (*i.e.* acceleration or deceleration of this change) has so far only been used to detect year-specific shifts in population trajectories (*10–12*).

While examining temporal changes in population abundance is valuable, understanding how these changes evolve over time, particularly in terms of their acceleration, offers deeper ecological insights. Here, the change in abundance over time (ΔN, eq. S14) reflects the net increase or decline in the number of individuals throughout a time series (i.e. linear trend of abundance over time), and the yearly growth rate (g, eq. S11) represents the average difference in absolute abundance from one year to the next. These differences are ecologically significant, as absolute bird numbers are linked to ecosystem services (*13*). Crucially, change in this growth rate (Δg, eq. S15) represents acceleration or deceleration in abundance change (Fig. 1). For instance, a negative Δg for a population already in decline (i.e. with negative ΔN) indicates an acceleration of the decline (Fig. 1). This second-order derivative remains largely unexplored in large-scale studies of biodiversity trends. Finally, an ecologically fundamental metric is the yearly per capita growth rate (r, eq. S12), along with its change through time (Δr, eq. S16), which captures how

individual contributions to population growth shift over time. Although Δg and Δr are related, they capture different ecological information: Δg reflects the magnitude of the acceleration in *absolute* numbers of birds and it thus reflects the shifting contribution of bird populations to ecosystems. In contrast, Δr is directly linked to underlying demographic processes of per-capita recruitment and loss, and it also provides a *relative* measure of acceleration comparable among populations of varying sizes.

Here, we provide a comprehensive assessment of temporal changes in local population abundances of 261 bird species across North America from 1987 to 2021, focusing on acceleration and deceleration. Using 1,033 routes of the North American Breeding Bird Survey (BBS, (*16*)), a long-term, annual, and standardized monitoring program, and advances in N-mixture population models (*14*, *15*), paired with full Bayesian inference, we demonstrate widespread bird abundance declines across North America, and pinpoint regions, taxa, and habitats where abundance declines accelerate or decelerate; we then show coincidence of the acceleration hotspots with environmental and anthropogenic variables. The time period of 1987 to 2021, though longer (*17*) or shorter (*18–20*) than in other studies on bird abundance changes in the US, balances long temporal coverage with broad spatial representation.

Nation-wide decline in abundance. The average change in total bird abundance per route (ΔN, eq. S14) is a significant decline of $\Delta N = -8.94$ individuals (95% Credible Interval $(CI) = [-10.01, -7.88]$, histogram in Fig. 2A), representing an average loss of 304 birds (out of an average abundance of 2,034 in 1987, *i.e.* 15%) per route from 1987 to 2021. The trends we uncover align with the reported decline of bird abundance across North America (*17*, *18*, *20*) and mirror trends in some European bird species (*21–27*). Of the 1,033 routes analyzed here, only 17% (172) experienced a significant increase in total bird abundance, while 70% (718) experienced a significant decrease (Fig. 2A, Figs. S1 and S2A). Using a spatial smoother to show average regional trends not obscured by local variation, we found only 7 routes located in regions with increasing abundance (dotted black circle Fig. 2B) and that bird abundances in Florida, Texas, Louisiana, and Arizona underwent the most pronounced average declines per route.

Regional hotspots of accelerating abundance decline. The average change of g per route is a significant decline with $\Delta g = -0.25$ ($CI = [-0.35, -0.16]$, histogram Fig. 2C), indicating that the yearly change in abundance (i.e. growth rate g) decreased over time (Fig. 2, C and D, Fig. S1, B and D, and Figs. S2A and S3A). That is, on average, routes experienced a significant acceleration of bird abundance decline. Among the 718 routes with significantly declining abundance, 163 routes exhibited a significant negative Δg and 146 a significant positive Δg (raw, not smoothed estimates, Fig. 2C).

Because the great majority of the spatially smoothed ΔN is negative (Fig. 2, B and D, outside the black dotted circle), the smoothed map of Δg can be interpreted as *average* regional acceleration ($\Delta g < 0$) and deceleration ($\Delta g > 0$) of the abundance decline (Fig. 2D, outside the black dotted circle, Fig. S1D). Parts of the Mid-Atlantic region of the US (Delaware, Maryland, and New Jersey), the Midwest (especially Indiana, Ohio, Kentucky, Illinois, Wisconsin, and Michigan), and California had negative smoothed Δg, indicating an acceleration of the decline in abundance (i.e., each year more birds are lost than in the previous year). In these regions, the gap between the number of lost and recruited individuals widens each year, raising concerns about the future of these bird populations. In contrast, the Yukon, Saskatchewan, Alberta, New Mexico, Alaska, Atlantic Canada (New Brunswick, Prince Edward Island, and Nova Scotia) Arizona, Montana, parts of New England (Massachusetts, Maine, New Hampshire, Vermont), Washington, Colorado, Oregon, South Carolina, and parts of Georgia and Northern Florida showed a positive smoothened Δg, that is a deceleration (i.e. slowdown) of the abundance decline. All raw spatial patterns of per capita growth rate change Δr were highly correlated with Δg (Spearman's correlation $= 0.97$, Fig. S4), but in contrast to the significant Δg, the average Δr at the continental scale was negative but with 95% CI overlapping zero (Figs. S3B, and S5). We suggest that this apparent discrepancy is because the mean Δr normalizes absolute change by abundance, allowing weak negative per capita trends to cause acceleration in total population decline.

Linking patterns of change to environment. We also investigated how raw and smoothed patterns of ΔN, Δg, and Δr correlate with environmental conditions. Changes in bird abundance have been previously linked to specific climates, habitats, land uses, and their temporal change. For instance, grassland and farmland species have been declining in both Europe and the US (*18*, *21–27*), while forest dwellers and species associated with warm climates have either remained stable or increased in some regions of Europe (*26–28*). Among the important processes previously linked to bird population dynamics are agricultural intensification (*21*, *23*, *26*, *29*, *30*) and changes in land-use (*21*, *22*). Here, we amassed 20 predictors representing either static patterns of climate, habitats, and human impact, or their temporal change, in North America, selected 12 of them to minimize collinearity (Fig. 3, Figs. S4 and S6, Table S1), and linked them to the raw and smoothed geographic patterns of ΔN, Δg and Δr using tree-based machine learning algorithms (Random Forest, Boosted Regression Tree, and XGBoost).

The first striking finding is that warm and warming regions coincide with areas of abundance decline (ΔN, Fig. 3, A and C, Figs. S7, and S8). This pattern is consistent with the evidence that bird populations are shifting their distributions northward as they track cooler conditions (*31*). Increases in temperatures have been shown to increase the risk of bird species' extinction due to a lack of species adaptability to rapidly changing climatic conditions (*32*), and consistent temperature-related responses have been documented across both Europe and North America (*33*). Our results further support this by showing that areas experiencing greater warming (Fig. 3C) also exhibit stronger abundance declines, suggesting that rising temperatures may be a driver of recent bird population losses.

The second major finding is that the hotspots of negative Δg (and Δr), i.e. the acceleration of the decline (Figs. 2D and S5B), coincide with areas of high-intensity agriculture, namely areas with high fertilizer use, high pesticide use, or large areas of croplands (*26*) (Fig. 3, B and D, Figs. S7, and S8). These three variables are strongly correlated (Fig. S4); thus, we cannot separate their independent effects, and we interpret them collectively as indicators of agricultural intensity. The coincidence between agricultural intensity and acceleration of bird abundance decline is concerning, especially given the increases in North American agricultural production, farm size, and mild increases in cropland area during the past 40 years (*34*).

We also found an interaction between agricultural intensity (i.e. pesticide use, fertilizer use and/or cropland area) and temperature change in their effect on Δg (Fig. S9): the negative effect of agricultural intensity on Δg is stronger in areas with more pronounced temperature increase. Indeed, agricultural landscapes are known to warm more than natural areas due to reduced vegetation cover and altered surface properties (*35*, *36*), which may amplify climate-driven stress on birds (*37*). Another possible explanation is that intense agricultural practices, through pesticide use and mechanical disturbance, interact with temperature change, further reducing food and habitat availability. Also, the non-linear effects of temperature on Δg (Fig. 3D) indicate that the strongest acceleration of decline occurs around intermediate mean temperatures (ca. 10°C), where bird populations are densest and human activities are most pronounced.

Clearly, the predictors for the acceleration differ from those driving the decline in abundance (ΔN) (Fig. 3, A and C, vs. B and D). This suggests that focusing only on the magnitude of the decline may underestimate the impact of agriculture on bird populations, as intense agriculture use can accelerate the abundance decline that may be primarily driven by climate. On the other hand, temperature change is the second most important variable explaining ΔN, Δg and Δr. The fact that we found similar relationships for changes in per capita growth rate (Δr, Fig. S10) suggests that agricultural intensity also affects not just total numbers, but also the increasing difference between individual survival and recruitment. Given the advances in the estimation of survival and recruitment from abundance time series (*14*, *15*, *38*), this is an opportunity for future research.

To our knowledge, this is the first large-scale study that has linked the acceleration of abundance change to the environment. Our findings suggest that such dynamics could represent a critical, yet unexplored, dimension of ecological responses: one that may yield valuable insights if applied to temporal dynamics of metrics such as species richness or turnover. Nonetheless, we also caution that this is a correlative post-hoc analysis, and that majority of geographic variation in ΔN, Δg, and Δr still remains to be explained. More robust causal analyses, such as quasi-causal analytical designs (*26*, *39*) or experiments (*40*, *41*) can help disentangle how agricultural practices impact abundance dynamics.

Per-species, per-family, and per-habitat analyses. In addition to the geographic variation in total ΔN, Δg, and Δr of all birds per route, we also assessed these metrics across all routes, and at different levels of taxonomic aggregation: species, family, and species' preferred habitat (*42*). Across 261 species, 84 species (32%) showed a significant positive ΔN, of which the majority (67 species) had a significant decelerating increase (Fig. 4A). This is expected, as a sustained accelerating increase in abundance is rapidly physically limited and therefore rare (*4*, *43*, *44*). In contrast, the most common trend was a significant decline, observed in 122 species (47%), with more than half of these (63 species, 53%) experiencing a significant acceleration of the decline (Fig. 4A). This indicates that most of the declining species, and a quarter of all the species analyzed, are undergoing a significant accelerating decline. Additionally, 21 families (39%) show a significant negative ΔN (vs. 14 positive), of which 10 experienced a significant acceleration of this decline (Fig. 4B). This indicates that most of the declining families are also experiencing an acceleration of the decline, showing that the pattern is not driven by a few taxonomic groups with shared traits or evolutionary histories, but is instead widespread across families. At the per capita level, while the number of species with negative Δr (67 species, Fig. S11B) was comparable to the number with negative Δg, only 7 species showed positive Δr. This indicates that, for most species undergoing declines in total abundance, the difference between per-capita recruitment and loss is widening. In contrast, species with positive ΔN showed only significant negative Δr, consistent with expectations under logistic growth as populations approach carrying capacity (Fig. S11B).

Out of 10 habitats considered here, only forests showed a significant positive ΔN, with a decelerating increase (Fig. 4C). Even though this increase seemingly contradicts the well-known decline in forest populations in the US (*17*, *18*, *20*), our classification is based on species' preferred habitats rather than biogeographic regions, as commonly used in previous studies. Consequently, our results of abundance decline across the contiguous US are consistent with those earlier findings, while the observed increase in forest specialists aligns with other analyses using similar habitat-based classifications in the US (*45*) and in Europe (*26*, *28*). Conversely, 4 habitats exhibited significant decline in abundance, with the strongest declines observed for towns, grasslands, marshes, and open woodlands (Fig. 4C, Fig. S12). Also, 2 of these habitats, namely marshes and open woodlands, showed an accelerating decline. These habitats are significantly impacted by human activities (*46–48*), suggesting a link between the acceleration of the decline and anthropogenic pressures such as agricultural intensification and habitat degradation. At the per capita level (Δr), patterns across families and preferred habitats were consistent with those observed for Δg (Fig. S11, C and D).

Conclusion. Using one of the most comprehensive and standardized bird time series datasets in the world, coupled with a state-of-the-art dynamic N-mixture Bayesian model, we examined the abundance dynamics and acceleration for 261 species over 35 years at a continental scale. While the hotspots of abundance decline coincide with warm and warming climates, the hotspots of accelerated decline coincide with agricultural intensity. These findings highlight the importance of monitoring not only ecological changes but also the second derivative of ecological variables over time. Incorporating acceleration of metrics into conservation assessments could uncover signals of decline that would remain hidden when focusing solely on abundance trends. Our approach could be applied to other taxa and biodiversity metrics, such as occupancy, species richness, or turnover, to test for similar acceleration patterns. Finally, our results are

concerning, particularly considering accelerating growth in human activities across various sectors such as economy, agriculture, or transportation (*4–6*, *49–52*).

Acknowledgements

This study stands on the shoulders of the thousands of volunteers who participated in the North American BBS, and the institutions that manage this program. The authors thank the Ohio Supercomputer Center for their computational resources. We thank all anonymous reviewers, Richard D. Gregory, and the editor Bianca Lopez, for their valuable comments and suggestion to perform correlative analyses. We thank Adam T. Clark, Florian Hartig, David Storch and Tomáš Telenský for valuable comments. **Funding:** F.L. and P.K. were funded by the European Union (ERC, BEAST, 101044740). Views and opinions expressed are however those of the author(s) only and do not necessarily reflect those of the European Union or the European Research Council Executive Agency. Neither the European Union nor the granting authority can be held responsible for them. M.A.J. was supported by the National Science Foundation DEB-1926598 and OISE-2330423. P.K. received funding from the Czech Science Foundation (project number: 24-14299L). **Author Contributions:** All authors conceived the idea of the paper; F.L, and P.K. conducted analyses; all authors wrote the paper. **Competing interest:** All authors declare no competing interests. **Data and materials availability:** All data and software are archived and available on Zenodo (*53*). No new materials were generated in this study.

References

1. IPBES, "Global assessment report on biodiversity and ecosystem services of the Intergovernmental Science-Policy Platform on Biodiversity and Ecosystem Services" (Zenodo, 2019); https://doi.org/10.5281/ZENODO.3831673.
2. C. T. Callaghan, L. Santini, R. Spake, D. E. Bowler, Population abundance estimates in conservation and biodiversity research. *Trends in Ecology & Evolution* **39**, 515–523 (2024).
3. J. Loh, R. E. Green, T. Ricketts, J. Lamoreux, M. Jenkins, V. Kapos, J. Randers, The Living Planet Index: using species population time series to track trends in biodiversity. *Philosophical Transactions of the Royal Society B: Biological Sciences* **360**, 289–295 (2005).
4. D. H. Meadows, Club of Rome, Eds., *The Limits to Growth: A Report for the Club of Rome's Project on the Predicament of Mankind* (Universe Books, New York, 1972).
5. T. Piketty, *Capital in the Twenty-First Century* (Harvard University Press, 2014; https://www.degruyter.com/document/doi/10.4159/9780674369542/html).
6. W. Steffen, W. Broadgate, L. Deutsch, O. Gaffney, C. Ludwig, The trajectory of the Anthropocene: The Great Acceleration. *The Anthropocene Review* **2**, 81–98 (2015).
7. A. D. Barnosky, N. Matzke, S. Tomiya, G. O. U. Wogan, B. Swartz, T. B. Quental, C. Marshall, J. L. McGuire, E. L. Lindsey, K. C. Maguire, B. Mersey, E. A. Ferrer, Has the Earth's sixth mass extinction already arrived? *Nature* **471**, 51–57 (2011).
8. G. Ceballos, P. R. Ehrlich, A. D. Barnosky, A. García, R. M. Pringle, T. M. Palmer, Accelerated modern human–induced species losses: Entering the sixth mass extinction. *Sci. Adv.* **1**, e1400253 (2015).
9. M. C. Urban, Accelerating extinction risk from climate change. *Science* **348**, 571–573 (2015).
10. A. C. Studeny, S. T. Buckland, P. J. Harrison, J. B. Illian, A. E. Magurran, S. E. Newson, Fine-tuning the assessment of large-scale temporal trends in biodiversity using the example of British breeding birds. *Journal of Applied Ecology* **50**, 190–198 (2013).
11. S. T. Buckland, A. E. Magurran, R. E. Green, R. M. Fewster, Monitoring change in biodiversity through composite indices. *Phil. Trans. R. Soc. B* **360**, 243–254 (2005).
12. R. M. Fewster, S. T. Buckland, G. M. Siriwardena, S. R. Baillie, J. D. Wilson, Analysis of population trends for farmland birds using Generalized Additive Models. *Ecology* **81**, 1970–1984 (2000).
13. K. J. Gaston, Birds and ecosystem services. *Current Biology* **32**, R1163–R1166 (2022).

14. D. Dail, L. Madsen, Models for Estimating Abundance from Repeated Counts of an Open Metapopulation. *Biometrics* **67**, 577–587 (2011).
15. M. Kéry, J. A. Royle, *Applied Hierarchical Modeling in Ecology: Analysis of Distribution, Abundance and Species Richness in R and BUGS: Volume 2: Dynamic and Advanced Models* (Academic Press, Cambridge, 1st edition., 2020).
16. D. Ziolkowski Jr., M. Lutmerding, V. Aponte, M.-A. Hudson, 2022 Release - North American Breeding Bird Survey Dataset (1966-2021), U.S. Geological Survey (2022); https://doi.org/10.5066/P97WAZE5.
17. A. Johnston, A. D. Rodewald, M. Strimas-Mackey, T. Auer, W. M. Hochachka, A. N. Stillman, C. L. Davis, V. Ruiz-Gutierrez, A. M. Dokter, E. T. Miller, O. Robinson, S. Ligocki, L. O. Jaromczyk, C. Crowley, C. L. Wood, D. Fink, North American bird declines are greatest where species are most abundant. *Science* **388**, 532–537 (2025).
18. K. V. Rosenberg, A. M. Dokter, P. J. Blancher, J. R. Sauer, A. C. Smith, P. A. Smith, J. C. Stanton, A. Panjabi, L. Helft, M. Parr, P. P. Marra, Decline of the North American avifauna. *Science* **366**, 120–124 (2019).
19. John R Sauer, William A Link, James E Hines, The North American Breeding Bird Survey, Analysis Results 1966 - 2019, U.S. Geological Survey (2020); https://doi.org/10.5066/P96A7675.
20. G. Dupont, A. Dobson, North American bird declines are driven by reductions in common species. *Sci. Adv.* **11**, eadw8971 (2025).
21. D. E. Bowler, H. Heldbjerg, A. D. Fox, M. De Jong, K. Böhning-Gaese, Long-term declines of European insectivorous bird populations and potential causes. *Conservation Biology* **33**, 1120–1130 (2019).
22. S. Fraixedas, A. Lindén, K. Meller, Å. Lindström, O. Keišs, J. A. Kålås, M. Husby, A. Leivits, M. Leivits, A. Lehikoinen, Substantial decline of Northern European peatland bird populations: Consequences of drainage. *Biological Conservation* **214**, 223–232 (2017).
23. C. A. Hallmann, R. P. B. Foppen, C. A. M. Van Turnhout, H. De Kroon, E. Jongejans, Declines in insectivorous birds are associated with high neonicotinoid concentrations. *Nature* **511**, 341–343 (2014).
24. R. Inger, R. Gregory, J. P. Duffy, I. Stott, P. Voříšek, K. J. Gaston, Common European birds are declining rapidly while less abundant species' numbers are rising. *Ecology Letters* **18**, 28–36 (2015).
25. I. Newton, The recent declines of farmland bird populations in Britain: an appraisal of causal factors and conservation actions. *Ibis* **146**, 579–600 (2004).
26. S. Rigal, V. Dakos, H. Alonso, A. Auniņš, Z. Benkő, L. Brotons, T. Chodkiewicz, P. Chylarecki, E. de Carli, J. C. del Moral, C. Domşa, V. Escandell, B. Fontaine, R. Foppen, R. Gregory, S. Harris, S. Herrando, M. Husby, C. Ieronymidou, F. Jiguet, J. Kennedy, A. Klvaňová, P. Kmecl, L. Kuczyński, P. Kurlavičius, J. A. Kålås, A. Lehikoinen, Å. Lindström, R. Lorrillière, C. Moshøj, R. Nellis, D. Noble, D. P. Eskildsen, J.-Y. Paquet, M. Pélissié, C. Pladevall, D. Portolou, J. Reif, H. Schmid, B. Seaman, Z. D. Szabo, T. Szép, G. T. Florenzano, N. Teufelbauer, S. Trautmann, C. van Turnhout, Z. Vermouzek, T. Vikstrøm, P. Voříšek, A. Weiserbs, V. Devictor, Farmland practices are driving bird population decline across Europe. *Proceedings of the National Academy of Sciences* **120**, e2216573120 (2023).
27. R. D. Gregory, M. A. Eaton, I. J. Burfield, P. V. Grice, C. Howard, A. Klvaňová, D. Noble, E. Šilarová, A. Staneva, P. A. Stephens, S. G. Willis, I. D. Woodward, F. Burns, Drivers of the changing abundance of European birds at two spatial scales. *Philosophical Transactions of the Royal Society B: Biological Sciences* **378**, 20220198 (2023).
28. R. D. Gregory, P. Vorisek, A. V. Strien, A. W. G. Meyling, F. Jiguet, L. Fornasari, J. Reif, P. Chylarecki, I. J. Burfield, Population trends of widespread woodland birds in Europe. *Ibis* **149**, 78–97 (2007).
29. R. E. Green, S. J. Cornell, J. P. W. Scharlemann, A. Balmford, Farming and the Fate of Wild Nature. *Science* **307**, 550–555 (2005).

30. R. L. Stanton, C. A. Morrissey, R. G. Clark, Analysis of trends and agricultural drivers of farmland bird declines in North America: A review. *Agriculture, Ecosystems & Environment* **254**, 244–254 (2018).
31. P. M. Martins, M. J. Anderson, W. L. Sweatman, A. J. Punnett, Significant shifts in latitudinal optima of North American birds. *Proc. Natl. Acad. Sci. U.S.A.* **121**, e2307525121 (2024).
32. C. H. Sekercioglu, S. H. Schneider, J. P. Fay, S. R. Loarie, Climate Change, Elevational Range Shifts, and Bird Extinctions. *Conservation Biology* **22**, 140–150 (2008).
33. P. A. Stephens, L. R. Mason, R. E. Green, R. D. Gregory, J. R. Sauer, J. Alison, A. Aunins, L. Brotons, S. H. M. Butchart, T. Campedelli, T. Chodkiewicz, P. Chylarecki, O. Crowe, J. Elts, V. Escandell, R. P. B. Foppen, H. Heldbjerg, S. Herrando, M. Husby, F. Jiguet, A. Lehikoinen, A. Lindstrom, D. G. Noble, J.-Y. Paquet, J. Reif, T. Sattler, T. Szep, N. Teufelbauer, S. Trautmann, A. J. van Strien, C. A. M. van Turnhout, P. Vorisek, S. G. Willis, Consistent response of bird populations to climate change on two continents. *Science* **352**, 84–87 (2016).
34. P. Potapov, S. Turubanova, M. C. Hansen, A. Tyukavina, V. Zalles, A. Khan, X.-P. Song, A. Pickens, Q. Shen, J. Cortez, Global maps of cropland extent and change show accelerated cropland expansion in the twenty-first century. *Nat Food* **3**, 19–28 (2021).
35. G. B. Bonan, Forests and Climate Change: Forcings, Feedbacks, and the Climate Benefits of Forests. *Science* **320**, 1444–1449 (2008).
36. S. Luyssaert, M. Jammet, P. C. Stoy, S. Estel, J. Pongratz, E. Ceschia, G. Churkina, A. Don, K. Erb, M. Ferlicoq, B. Gielen, T. Grünwald, R. A. Houghton, K. Klumpp, A. Knohl, T. Kolb, T. Kuemmerle, T. Laurila, A. Lohila, D. Loustau, M. J. McGrath, P. Meyfroidt, E. J. Moors, K. Naudts, K. Novick, J. Otto, K. Pilegaard, C. A. Pio, S. Rambal, C. Rebmann, J. Ryder, A. E. Suyker, A. Varlagin, M. Wattenbach, A. J. Dolman, Land management and land-cover change have impacts of similar magnitude on surface temperature. *Nature Clim Change* **4**, 389–393 (2014).
37. K. S. Lauck, A. Ke, E. M. Olimpi, D. Paredes, K. Hood, T. Phillips, W. R. L. Anderegg, D. S. Karp, Agriculture and hot temperatures interactively erode the nest success of habitat generalist birds across the United States. *Science* **382**, 290–294 (2023).
38. E. Bellier, M. Kéry, M. Schaub, Simulation-based assessment of dynamic *N* -mixture models in the presence of density dependence and environmental stochasticity. *Methods Ecol Evol* **7**, 1029–1040 (2016).
39. A. T. Clark, H. Ye, F. Isbell, E. R. Deyle, J. Cowles, G. D. Tilman, G. Sugihara, Spatial convergent cross mapping to detect causal relationships from short time series. *Ecology* **96**, 1174–1181 (2015).
40. R. B. Bradbury, A. Kyrkos, A. J. Morris, S. C. Clark, A. J. Perkins, J. D. Wilson, Habitat associations and breeding success of yellowhammers on lowland farmland. *Journal of Applied Ecology* **37**, 789–805 (2000).
41. J. A. Vickery, J. R. Tallowin, R. E. Feber, E. J. Asteraki, P. W. Atkinson, R. J. Fuller, V. K. Brown, The management of lowland neutral grasslands in Britain: effects of agricultural practices on birds and their food resources. *Journal of Applied Ecology* **38**, 647–664 (2001).
42. Cornell Lab of Ornithology, All About Birds (2019). https://www.allaboutbirds.org.
43. G. E. Hutchinson, *An Introduction to Population Ecology* (Yale Univ. Pr, New Haven, 4. print., 1979).
44. L. L. Rockwood, *Introduction to Population Ecology* (John Wiley & Sons, Incorporated, Newark, 1st ed., 2015)*New York Academy of Sciences Series*.
45. S. J. Murphy, M. A. Jarzyna, Spatial and temporal non-stationarity in long-term population dynamics of over-wintering birds of North America. *Ecology and Evolution* **13**, e9781 (2023).
46. L. A. Brennan, W. P. Kuvlesky, North american grassland birds: an unfolding conservation crisis? *Journal of Wildlife Management* **69**, 1–13 (2005).
47. J. M. Marzluff, "Worldwide urbanization and its effects on birds" in *Avian Ecology and Conservation in an Urbanizing World*, J. M. Marzluff, R. Bowman, R. Donnelly, Eds. (Springer US, Boston, MA, 2001; http://link.springer.com/10.1007/978-1-4615-1531-9_2), pp. 19–47.

48. N. C. Davidson, How much wetland has the world lost? Long-term and recent trends in global wetland area. *Mar. Freshwater Res.* **65**, 934 (2014).
49. K. C. Seto, B. Güneralp, L. R. Hutyra, Global forecasts of urban expansion to 2030 and direct impacts on biodiversity and carbon pools. *Proc. Natl. Acad. Sci. U.S.A.* **109**, 16083–16088 (2012).
50. D. Tilman, J. Fargione, B. Wolff, C. D'Antonio, A. Dobson, R. Howarth, D. Schindler, W. H. Schlesinger, D. Simberloff, D. Swackhamer, Forecasting Agriculturally Driven Global Environmental Change. *Science* **292**, 281–284 (2001).
51. J. A. Foley, N. Ramankutty, K. A. Brauman, E. S. Cassidy, J. S. Gerber, M. Johnston, N. D. Mueller, C. O'Connell, D. K. Ray, P. C. West, C. Balzer, E. M. Bennett, S. R. Carpenter, J. Hill, C. Monfreda, S. Polasky, J. Rockström, J. Sheehan, S. Siebert, D. Tilman, D. P. M. Zaks, Solutions for a cultivated planet. *Nature* **478**, 337–342 (2011).
52. E. C. Ellis, K. Klein Goldewijk, S. Siebert, D. Lightman, N. Ramankutty, Anthropogenic transformation of the biomes, 1700 to 2000. *Global Ecology and Biogeography* **19**, 589–606 (2010).
53. F. Leroy, P. Keil, Zenodo Version 1.0.6, version v1.0.6, Zenodo (2025); https://zenodo.org/doi/10.5281/zenodo.18085017.
54. J. A. Royle, N-Mixture Models for Estimating Population Size from Spatially Replicated Counts. *Biometrics* **60**, 108–115 (2004).
55. E. Bellier, M. Kéry, M. Schaub, Relationships between vital rates and ecological traits in an avian community. *Journal of Animal Ecology* **87**, 1172–1181 (2018).
56. M. Kéry, J. A. Royle, *Applied Hierarchical Modeling in Ecology: Analysis of Distribution, Abundance and Species Richness in R and BUGS: Volume 1:Prelude and Static Models* (Academic Press, Amsterdam ; Boston, 1st edition., 2015).
57. S. T. Buckland, D. R. Anderson, K. P. Burnham, J. L. Laake, D. L. Borchers, L. Thomas, *Advanced Distance Sampling* (Oxford University PressOxford, 2004; https://academic.oup.com/book/53875).
58. S. T. Buckland, D. R. Anderson, K. P. Burnham, J. L. Laake, D. L. Borchers, L. Thomas, *Introduction to Distance Sampling: Estimating Abundance of Biological Populations* (Oxford University PressOxford, 2001; https://academic.oup.com/book/53746).
59. M. Plummer, JAGS: A program for analysis of Bayesian graphical models using Gibbs sampling. In K. Hornik, F. Leisch, & A. Zeileis (Eds.), Proceedings of the 3rd International Workshop on Distributed Statistical Computing, 124(125.10), 1–10. (2003).
60. K. Kellner, *jagsUI: A Wrapper Around "rjags" to Streamline "JAGS" Analyses* (2021; https://CRAN.R-project.org/package=jagsUI).
61. R Core Team, *R: A Language and Environment for Statistical Computing* (R Foundation for Statistical Computing, Vienna, Austria, 2021; https://www.R-project.org/).
62. A. Gelman, D. B. Rubin, Inference from Iterative Simulation Using Multiple Sequences. *Statist. Sci.* **7** (1992).
63. W. Viechtbauer, Conducting Meta-Analyses in *R* with the **metafor** Package. *J. Stat. Soft.* **36** (2010).
64. S. N. Wood, Fast stable restricted maximum likelihood and marginal likelihood estimation of semiparametric generalized linear models. *Journal of the Royal Statistical Society (B)* **73**, 3–36 (2011).
65. C. M. Wieben, Preliminary estimated annual agricultural pesticide use for counties of the conterminous United States, 2018, U.S. Geological Survey (2021); https://doi.org/10.5066/P920L09S.
66. U.S. Geological Survey, Estimated annual agricultural pesticide use by county for the conterminous United States, 1992–2018, U.S. Geological Survey (2025); https://water.usgs.gov/nawqa/pnsp/usage/maps/index.php.
67. L. M. Guzman, E. Elle, L. A. Morandin, N. S. Cobb, P. R. Chesshire, L. M. McCabe, A. Hughes, M. Orr, L. K. M'Gonigle, Impact of pesticide use on wild bee distributions across the United States. *Nat Sustain* **7**, 1324–1334 (2024).
68. L. Breiman, Random Forests. *Machine Learning* **45**, 5–32 (2001).
69. J. Elith, J. R. Leathwick, T. Hastie, A working guide to boosted regression trees. *Journal of Animal Ecology* **77**, 802–813 (2008).

70. T. Chen, C. Guestrin, “XGBoost: A Scalable Tree Boosting System” in *Proceedings of the 22nd ACM SIGKDD International Conference on Knowledge Discovery and Data Mining* (Association for Computing Machinery, New York, NY, USA, 2016; https://doi.org/10.1145/2939672.2939785)*KDD ’16*, pp. 785–794.
71. M. N. Wright, A. Ziegler, ranger: A Fast Implementation of Random Forests for High Dimensional Data in C++ and R. *Journal of Statistical Software* **77**, 1–17 (2017).
72. G. Ridgeway, G. Developers, gbm: Generalized Boosted Regression Models, (2003); https://doi.org/10.32614/CRAN.package.gbm.
73. T. Chen, T. He, M. Benesty, V. Khotilovich, Y. Tang, H. Cho, K. Chen, R. Mitchell, I. Cano, T. Zhou, M. Li, J. Xie, M. Lin, Y. Geng, Y. Li, J. Yuan, xgboost: Extreme Gradient Boosting, (2014); https://doi.org/10.32614/CRAN.package.xgboost.
74. D. Zanaga, R. Van De Kerchove, W. De Keersmaecker, N. Souverijns, C. Brockmann, R. Quast, J. Wevers, A. Grosu, A. Paccini, S. Vergnaud, O. Cartus, M. Santoro, S. Fritz, I. Georgieva, M. Lesiv, S. Carter, M. Herold, L. Li, N.-E. Tsendbazar, F. Ramoino, O. Arino, ESA WorldCover 10 m 2020 v100, version v100, Zenodo (2021); https://doi.org/10.5281/ZENODO.5571936.
75. M. Zhao, S. W. Running, Drought-Induced Reduction in Global Terrestrial Net Primary Production from 2000 Through 2009. *Science* **329**, 940–943 (2010).
76. R. J. Hijmans, S. E. Cameron, J. L. Parra, P. G. Jones, A. Jarvis, Very high resolution interpolated climate surfaces for global land areas. *Int. J. Climatol.* **25**, 1965–1978 (2005).
77. H. I. Reuter, A. Nelson, A. Jarvis, An evaluation of void-filling interpolation methods for SRTM data. *International Journal of Geographical Information Science* **21**, 983–1008 (2007).
78. N. J. L. Lenssen, G. A. Schmidt, J. E. Hansen, M. J. Menne, A. Persin, R. Ruedy, D. Zyss, Improvements in the GISTEMP Uncertainty Model. *JGR Atmospheres* **124**, 6307–6326 (2019).
79. N. Lenssen, G. A. Schmidt, M. Hendrickson, P. Jacobs, M. J. Menne, R. Ruedy, A NASA GISTEMPv4 Observational Uncertainty Ensemble. *JGR Atmospheres* **129**, e2023JD040179 (2024).
80. P. Potter, N. Ramankutty, E. M. Bennett, S. D. Donner, Characterizing the Spatial Patterns of Global Fertilizer Application and Manure Production. *Earth Interactions* **14**, 1–22 (2010).
81. K. C. GUAY, P. S. A. BECK, S. J. GOETZ, Long-Term Arctic Growing Season NDVI Trends from GIMMS 3g, 1982-2012. ORNL Distributed Active Archive Center [Preprint] (2015). https://doi.org/10.3334/ORNLDAAC/1275.
82. O. Venter, E. W. Sanderson, A. Magrach, J. R. Allan, J. Beher, K. R. Jones, H. P. Possingham, W. F. Laurance, P. Wood, B. M. Fekete, M. A. Levy, J. E. M. Watson, Global terrestrial Human Footprint maps for 1993 and 2009. *Sci Data* **3**, 160067 (2016).
83. Center For International Earth Science Information Network-CIESIN-Columbia University, Documentation for the Gridded Population of the World, Version 4 (GPWv4), Revision 11 Data Sets. Palisades, NY: NASA Socioeconomic Data and Applications Center (SEDAC) [Preprint] (2018). https://doi.org/10.7927/H45Q4T5F.

Supplementary materials

Materials and Methods
Figs. S1 to S14
Table S1
References (54-83)

Figures

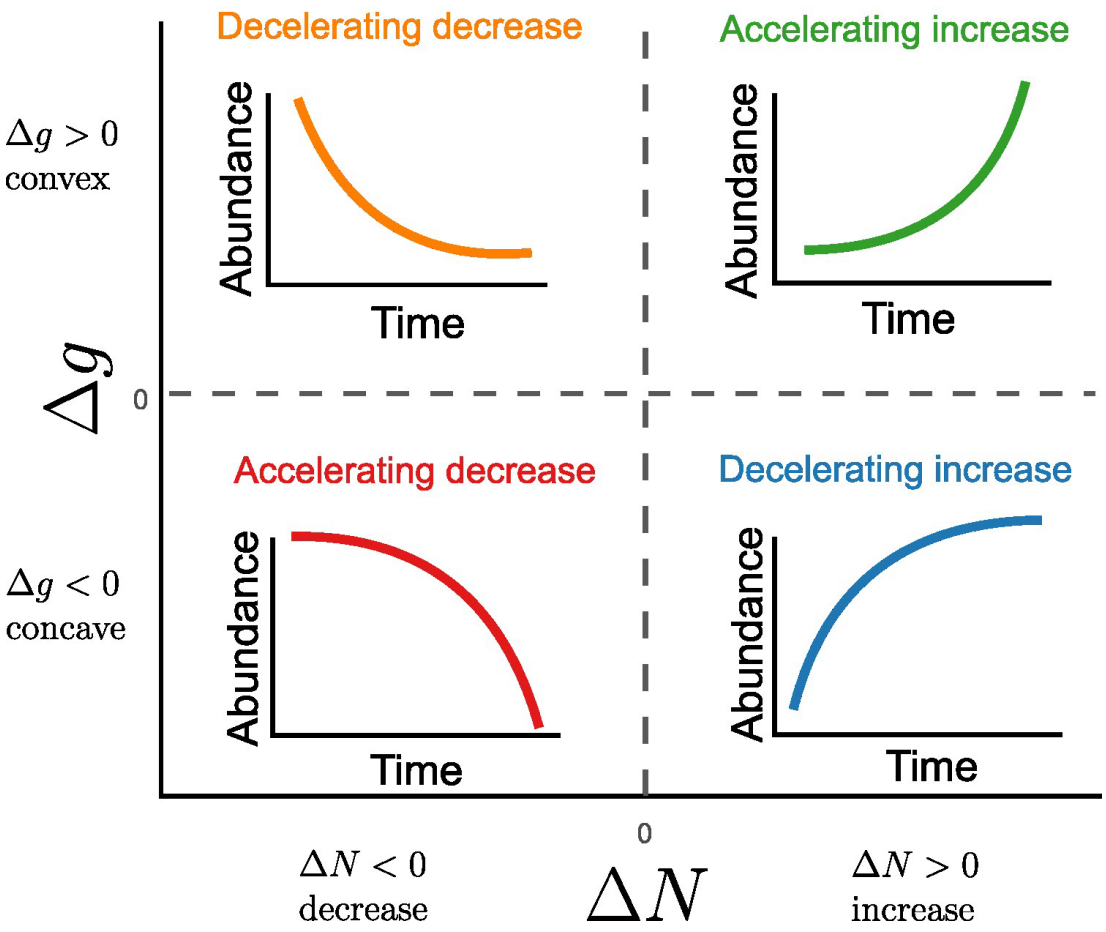

Fig. 1 | Illustration of acceleration and deceleration of abundance change. Here, ΔN denotes abundance change, and Δg (change in yearly growth rate) its acceleration or deceleration. The case where $\Delta g = 0$ represents a constant rate of change, that is, no acceleration or deceleration in ΔN (i.e. linear trend).

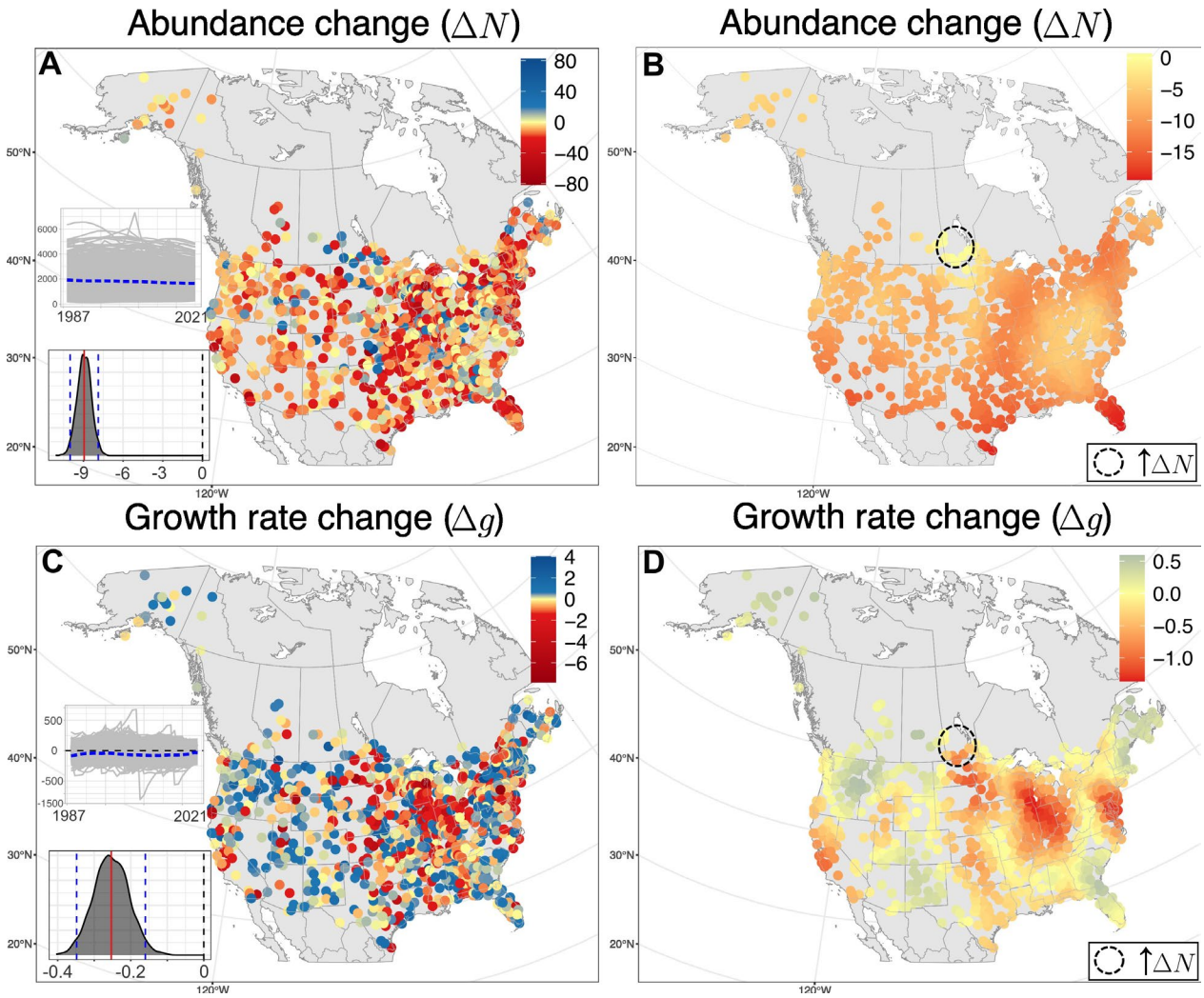

Fig. 2 | Temporal change of abundance and growth rate. (**A** and **B**) Total changes in bird abundance per route from 1987 to 2021 (ΔN), and (**C** and **D**) temporal change of growth rate (Δg), after correcting for imperfect detection. Maps in panels (**B** and **D**) are estimates from the dynamic *N*-mixture models, smoothed using a spatial GAM (total var. explained R^2 are 7.62% and 16.5% respectively); non-smoothed values are in panels (**A** and **C**). Smoothed and non-smoothed panels share the same fixed color scale. Since abundance is decreasing across most of North America, the red regions in panel (**D**) are regional hotspots of acceleration of bird abundance decline. Dashed circles in (**B** and **D**) mark the only region with positive values of the smoothed ΔN. Inset plots in bottom left show the raw (i.e. not spatially smoothed) changes in abundance and growth rate with the average trend in blue dashed line; y-axes in (**C**) are signed square root transformed. The histograms show the posterior distributions of the average slope; red vertical lines are means and dashed blue lines are 95% credible intervals.

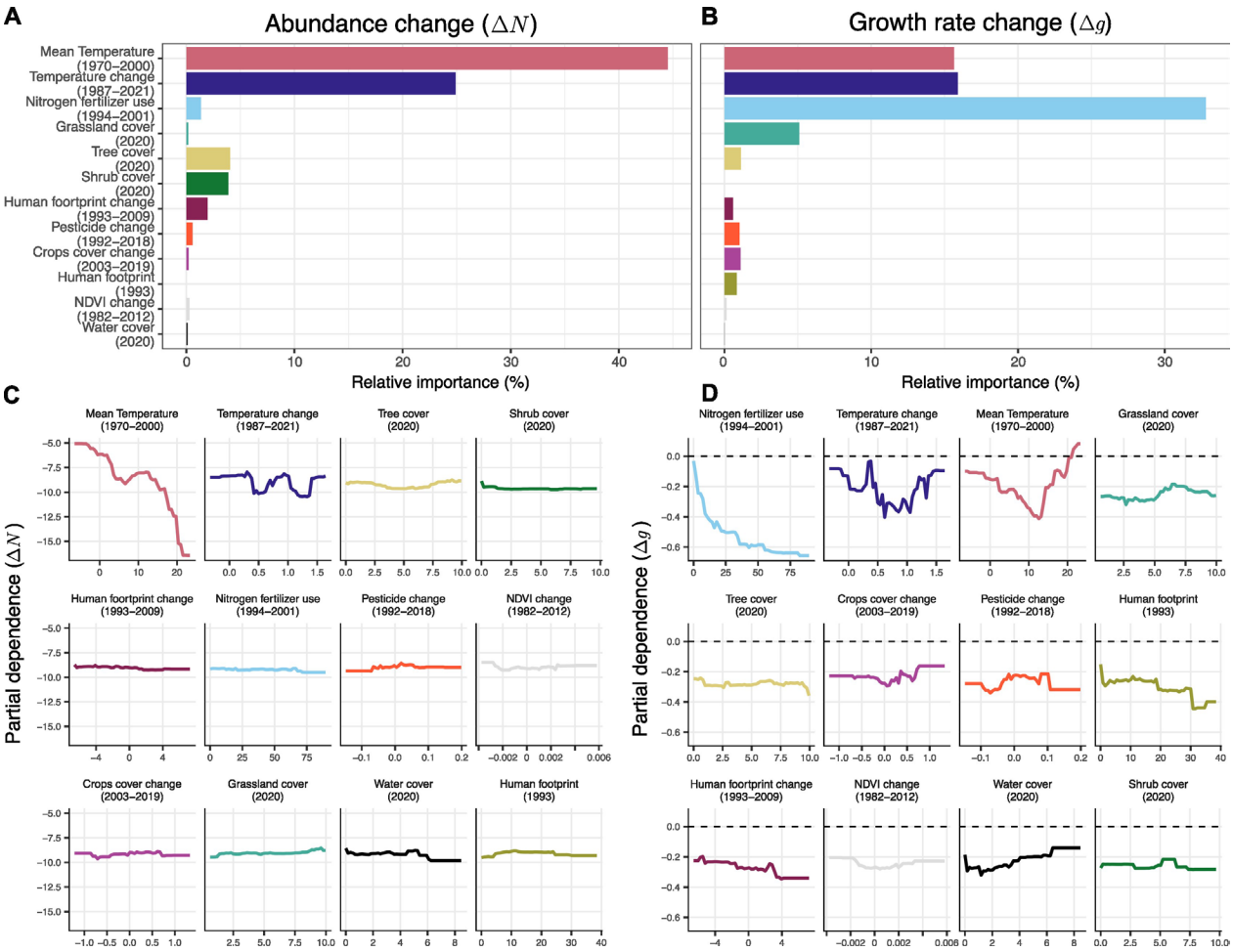

Fig. 3 | Variable importances (A and B) and partial dependence plots (C and D) from best performing tree-based models explaining changes in spatially smoothed abundance change ΔN and growth rate change Δg. (**A** and **B**) Variable importance scores scaled to R^2 from XGBoost for ΔN (total var. explained $R^2 = 82.9\%$), and for Δg (total var. explained $R^2 = 75.2\%$). (**C** and **D**) Partial dependence plots ordered from most to least important predictors, for ΔN and Δg, respectively. Note here that more negative values of Δg indicate accelerated declines in abundance.

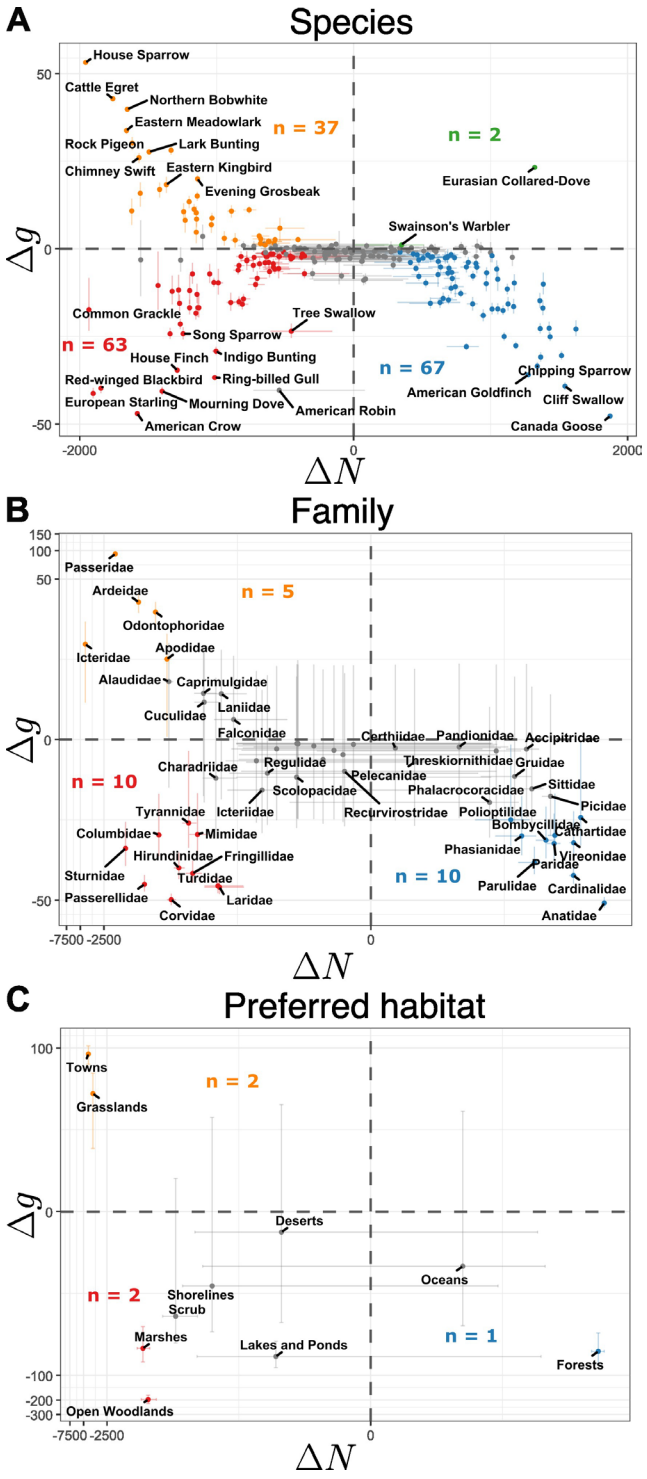

Fig. 4 | Acceleration and deceleration of bird abundance change aggregated across species, families, and habitats. Each point represents ΔN and Δg calculated by aggregating all individuals at the level of (**A**) a species, (**B**) a family, and (**C**) a habitat. Error bars show the 95% credible intervals (CI), and grey points indicate non-significant acceleration or deceleration (i.e. 95% CI overlaps 0 on either axis). Colors follow Fig. 1's scheme (red = accelerating decrease; orange = decelerating decrease; blue = decelerating increase; green = accelerating increase). The number (n) of significant points in each quadrant is noted. Axes are pseudo log-transformed for better visual separation.

Science
AAAS

Supplementary Materials for

Acceleration hotspots of North American birds' decline are associated with agriculture

François Leroy*, Marta A. Jarzyna, Petr Keil

*Correspondence to: leroy@fzp.czu.cz

This PDF file includes:

Materials and Methods

Data. To investigate patterns of population dynamics of birds in North America, we used the North American Breeding Bird Survey (*16*) (hereafter BBS), an ongoing bird monitoring initiative launched in 1966. Spanning more than 50 years, the BBS comprises 39.2 km-long routes scattered across the contiguous United States and Canada, each divided into 50 census points at approximately 800 m intervals. From its inception with about 500 routes in 1966, the BBS has grown to encompass 5,581 routes by 2021. At the time of our data download on September 5, 2022, the data contained 6,946,871 records of species abundances compiled by 10,316 volunteers for 746 species and spanning over 50 years. The BBS data also contains meteorological data, date, hour, and spatial coordinates.

Routes with long time-series (e.g. from 1969 to 2021) were spatially sparse. To balance long temporal extent with robust spatial coverage, we focused our analysis on the 1987-2021 period and selected routes with no more than 15 years of missing data. This timeframe, although longer than (*17*) and shorter than (*18–20*), balances long temporal coverage with broad spatial representation.

For each species, we extracted the preferred habitat from the eBird/Cornell online database (*42*). These were: Towns, Grasslands, Shorelines, Scrubs, Deserts, Rivers and Streams, Marshes, Open Woodlands, Forests, Lakes and Ponds, Oceans, and Tundra. Species with missing habitat data (23 in total) were excluded. In the end, we performed our analysis using 1,033 routes from 1987 to 2021 (*i.e.* 35 years), with 1,623,394 occurrences of 564 species.

Dynamic *N*-mixture model. We modelled the abundance of each of the 564 bird species across each route and year from 1987 to 2021 using a dynamic *N*-mixture model (*14*), hereafter the DM model (Dail & Madsen, 2011). It is a generalization of the *N*-mixture model by Royle (*54*) that assumes open populations (*i.e.* metapopulations can experience births, immigrations, deaths, or emigrations) and that has been successfully applied to data similar to the BBS (*14*, *15*). While the DM model can accommodate repeated counts, we did not use them primarily for computational feasibility (*15*).

Important features of the model are that (i) it can account for imperfect detectability of individuals and was shown to be very robust at predicting abundance and growth rate (*13*, *14*, *37*, *55*, Fig. S14), (ii) it can estimate recruitment and survival rates merely from abundance counts. The latter may seem counterintuitive to some, and we refer those readers to (*14*) and (*15*) for details on how this works. However, while the model tends to overestimate survival and underestimate recruitment, it has nonetheless demonstrated superior performance compared to alternative approaches for estimating abundance from single-count data (*15*, *38*, *55*). Note that the DM model assumes that all birds around a point are equally detectable, irrespectively of the distance from the observer (unlike (*56–58*)). This may lead to underestimation of abundance. However, since this assumption is constant over years, and thanks to the standardized sampling BBS protocol, the model should provide reliable inference about the relative abundance over time (*15*), in line with the goals of this study.

The exact definition of the model is as follows: For a species j and a route i, the abundance at time $t+1$ (*i.e.* $N_{j,i,t+1}$) is the sum of surviving individuals ($S_{j,i,t+1}$) from the previous year and newly recruited individuals ($R_{j,i,t+1}$):

$$N_{j,i,t+1} = S_{j,i,t+1} + R_{j,i,t+1} \quad \text{eq. S1}$$

Survival and recruitment are modeled separately. The number of surviving individuals $S_{j,i,t+1}$, is assumed to follow a Binomial distribution:

$$S_{j,i,t+1} \sim Binomial(N_{j,i,t}, \phi_{j,i,t}) \quad \text{eq. S2}$$

Where $N_{j,i,t}$ is the abundance of species j at route i and time t, and $\phi_{j,i,t}$ is the probability that an individual survives from t to $t+1$.

Similarly, recruitment $R_{j,i,t+1}$, follows a Poisson distribution:

$$R_{j,i,t+1} \sim Poisson(\gamma_{j,i,t}) \quad \text{eq. S3}$$

where $\gamma_{j,i,t}$ is the expected number of recruited individuals. The abundance at time 1 ($N_{j,i,1}$) is:

$$N_{j,i,1} \sim Poisson(\lambda_{j,i,1}), \quad \text{eq. S4}$$

where $\lambda_{j,i,1}$ is the mean abundance of the species j at route i at time 1.

To correct for imperfect detection, the *observed* count ($C_{j,i,t}$) is modelled as a Binomial random variable, conditional on the true abundance ($N_{j,i,t}$):

$$C_{j,i,t} \sim Binomial(N_{j,i,t}, p_{j,i,t}) \quad \text{eq. S5}$$

Here, $p_{j,i,t}$ is the species-specific probability of detecting an individual. The detection probability is modelled on the logit scale:

$$logit(p_{j,i,t}) = \alpha + \boldsymbol{x}_{j,i,t}^{\intercal}\boldsymbol{b}, \quad \text{eq. S6}$$

where α is the intercept, $\boldsymbol{x}^{\intercal}$ is the transpose of a vector of covariates, and $\boldsymbol{b}$ is a vector of regression coefficients. The covariates $\boldsymbol{x}$ include: the exact time of the day of the census (in decimal hours), and weather data, *i.e.* wind condition (ordinal variable with 9 levels ranging from < 2 km.h^{-1} to 74 km.h^{-1}), sky condition (factor with 7 levels: clear sky, partly cloudy, cloudy, fog, drizzle, snow, and shower), and average temperature during the census (in °C). Missing values for the time of the day and temperature were imputed following Kéry and Royle (2015), by sampling from a normal distribution:

$$x_{i,t} \sim N(\mu, \sigma) \text{ eq. S7}$$

where μ and σ are means and variance of observed data for the respective covariate. An implementation of the model in JAGS programming language (*59*) is in the Zenodo repository (*53*).

Following Kéry and Royle (2020) implementation, λ, γ, and ϕ were modelled as an intercept (α) as follows:

$$\log(\lambda_{i,1}) = \alpha.\lambda \quad \text{eq. S8}$$

$$\log(\gamma_{i,t}) = \alpha.\gamma \quad \text{eq. S9}$$

$$\text{logit}(\phi_{i,t}) = \alpha.\phi \quad \text{eq. S10}$$

Here $\alpha.\lambda$, $\alpha.\gamma$, and $\alpha.\phi$ come from wide Normal prior distributions $N(0,100)$, with 100 being the variance of the normal distribution.

Model fitting. For each *j*-th species, we fitted the DM model in a Bayesian framework using MCMC sampler JAGS (Plummer, 2003; https://mcmc-jags.sourceforge.io/), interfaced through the package jagsUI (*60*) in R ver. 4.2.1 (*61*). For all the parameters, we used normal distributions with 0 mean and variance of 100 (Appendix B). The settings for the MCMC algorithm were: 3 chains, 200,000 iterations per chain, 75,000 burn-in, a thinning rate of 100, and 1,000 iterations in the adaptative phase. The entire fitting procedure for all 564 species (1 core per MCMC chain, 3 chains per species) required approximately 2 days on 1,692 cores of the Ohio Supercomputer Center (https://www.osc.edu/), each core operating at 2.5 GHz.

Convergence diagnostics. We assessed the convergence of the DM models for each species by computing the $\hat{R}$ (Rhat, Gelman & Rubin, 1992) for all of the parameters of the model. Following standard practice (Gelman & Rubin, 1992), we only retained the most reliable models with all parameters $\hat{R} \leq 1.1$, which led to a final set of 261 species for further analysis (Fig. S13). The reduction from the initial 564 species reflects the complexity of the DM model, which can lead to the unidentifiability of certain parameters in some models, especially for rare species with limited presence and low abundance. We also visually inspected the estimated and predicted abundance (Fig. S14).

Demographic rates. From the output of the DM model and for each *j*-th species at *i*-th site and *t*-th year (starting from 1988), we derived the **yearly growth rate** $g_{j,i,t+1}$:

$$g_{j,i,t+1} = \frac{N_{j,i,t+1} - N_{j,i,t}}{\Delta t} = N_{j,i,t+1} - N_{j,i,t} \qquad \text{eq. S11}$$

where Δt is the time between t and $t+1$; in our case $\Delta t = 1$ year.

We also calculated the intrinsic **yearly per capita growth rate** $r_{j,i,t+1}$:

$$r_{j,i,t+1} = \frac{N_{j,i,t+1} - N_{j,i,t}}{N_{j,i,t}} = \frac{g_{j,i,t+1}}{N_{j,i,t}} \qquad \text{eq. S12}$$

Per route, per species, per family and per habitat analyses. We assessed all metrics at different levels of taxonomic aggregation. First, for each route, we aggregated the number of individuals of all the species together and assessed aggregated abundance and growth rate. Conversely, for each species, family or preferred habitat, we aggregated those metrics over all the routes. In other words, these were not mapped geographically as in the spatial analysis, but the numbers were aggregated for each grouping (species, family, habitat) over all 1,033 routes included in our analysis.

In the DM model, each value of $N_{j,i,t}$, for each species j, site i, and time t is estimated with a posterior distribution. To propagate the uncertainty of these estimates to the higher levels of aggregations (namely route, family and preferred habitat), we sampled each of those posterior distributions 500 times. For each sample, we aggregated those values per route, species, family or preferred habitat. This gave us a new posterior distribution of N, with a mean ($y_{j,t}$) and standard deviation ($sd_{j,t}$) at the desired level of aggregation. We performed the same propagation of uncertainty for the rates g, across all the levels of aggregation. Because these values are derived from posterior distributions, the reported means and credible intervals are not restricted to

integers even though the underlying counts are discrete. Retaining these values without rounding avoids potential rounding artifacts.

Temporal change with Bayesian mixed models. We assessed the temporal change of the estimated N, g and r for the different levels of aggregation while propagating the uncertainty of these estimates from the posteriors of the DM model, using mixed models. We used a random varying slope and intercept for each route, species, family or preferred habitat (j):

$$y_{j,t} = \Delta y_j \times t + \beta_{0_j} + \epsilon_{j,t} \quad \text{eq. S13}$$

By substituting $N_{j,t}$ into $y_{j,t}$, we get the **abundance change** (ΔN_j):

$$\Delta N_j = \frac{N_{j,t} - \beta_{0_j} - \epsilon_{j,t}}{t} \quad \text{eq. S14}$$

It measures the linear trend of abundance over the whole time series. This is a simplification; we are aware that trends of abundance are often non-linear (e.g. Fig. S12A). The reason for measuring the linear trend is to see if there is an overall decline or increase. Systematic deviations from this linear trend (acceleration or deceleration) are then captured by the Δg and Δr below. Alternatively, abundance change can be estimated as a slope of a generalized linear model of N_t against t, with Poisson errors and log link. However, since this gives similar hotspots of decline as the linear model (*53*), and since eq. S14 is interpretable in numbers of individual birds, we prefer eq. S14.

By substituting $g_{j,t}$ into $y_{j,t}$, we get the **growth rate change** (Δg_j):

$$\Delta g_j = \frac{g_{j,t} - \beta_{0_j} - \epsilon_{j,t}}{t} \quad \text{eq. S15}$$

It measures the acceleration or deceleration of the yearly growth rate.

By substituting $r_{j,t}$ into $y_{j,t}$, we get the **per capita growth rate change** (Δr_j):

$$\Delta r_j = \frac{r_{j,t} - \beta_{0_j} - \epsilon_{j,t}}{t} \quad \text{eq. S16}$$

Note that β_{0_j} and $\epsilon_{j,t}$ are not the same for eqs. 14-16, they are estimated independently for each metric; we use the same notation for convenience.

We obtained each $y_{j,t}$ as the mean of the posterior distribution (see previous paragraph) estimated by the DM model, Δy_j and β_{0_j} are the random slopes and intercepts, j is the index of the level of aggregation (e.g. j-th route) and t the year in the time series. The error term $\epsilon_{j,t}$ comes from a normal distribution

$$\epsilon_{j,t} \sim N(0, sd_{j,t}), \quad \text{eq. S17}$$

where $sd_{j,t}$ is the standard deviation of the posterior distribution of $y_{j,t}$ estimated in the DM model (see previous paragraph). This way, the per-species uncertainty of all the y metrics (estimated in the DM model) is propagated to the mixed effect model of temporal change, an approach used in meta analyses (*63*). Finally, the random slopes Δy_j and intercepts β_{0_j} come from normal distributions:

$$\Delta y_j \sim N\left(M_{\Delta y}, SD_{\Delta y}\right) \quad \text{eq. S18}$$

$$\beta_{0_j} \sim N\left(M_{\beta_0}, SD_{\beta_0}\right) \quad \text{eq. S19}$$

The posterior distributions of $M_{\Delta y}$ and M_{β_0} represent the grand means of the change and describe the overall temporal change across all *j*s.

We provided uninformative priors for both M and SD as follows:

$$M \sim N(0, 10^{100}) \quad \text{eq. S20}$$

$$SD \sim Unif(0, 100) \quad \text{eq. S21}$$

Spatial smoothing. For the spatial analysis, mapping the above-mentioned temporal changes (ΔN, Δg, Δr) may reveal a substantial local variation among individual routes, which could obscure average trends across larger regions. To detect these regional anomalies, we smoothed the variation of the rates using spatial generalized additive models (GAM) using the R package mgcv (*64*):

$$\Delta y_j = \mathrm{s}\left(Lon_j, Lat_j\right), \quad \text{eq. S22}$$

with Δy_j the temporal change of the metric considered at route j, Lon and Lat the longitude and latitude of the route j, and $s()$ indicating that longitude and latitude are treated as interacting covariates in the spline function of the smoother. For the spline function, we used a gaussian process as a smooth class (argument "bs" of the $s()$ function in mgcv) with 100 basis functions (approximately $\frac{1}{10}^{th}$ of the number of routes).

Linking patterns of change to environment. To interpret the patterns of acceleration, we performed a post-hoc analysis of coincidence between hotspots of ΔN, Δg (Fig. 2), and Δr (Fig. S5) with several environmental and human-related variables. We obtained rasterized data on land cover, cropland area and its temporal change, fertilizer usage, vegetation greenness and its change, net primary productivity, climate, temperature change, human footprint and its temporal change, human population density, and elevation (Table S1). We aggregated some of these rasters to a coarser resolution (mostly those which originally came at a 30 sec resolution) to better represent regional means, since the smoothened demographic rates also represent regional means. The original and coarsened resolutions are listed in Table S1. The aggregation function was either sum (for areas of land cover classes and cropland area) or arithmetic mean (for the rest of variables).

We also downloaded shapefiles of pesticide use from USGS NAWQA (*65*, *66*) from 1992 to 2018 at the county level over the contiguous US. We selected the 182 compounds that were reported consistently for all years from 1992 to 2018. Following (*67*), we computed:

$$\text{pesticide use} = log\left(\frac{\sum \text{kg of pesticide}}{\text{county area}}\right) \quad \text{eq. S23}$$

We then averaged pesticide use (eq. S23) over the entire time period from 1992 to 2018 for every county and obtained the average pesticide use per square meter (Fig. S6). We also assessed the

change in pesticide use per county from a linear regression between pesticide use (eq. S23) and time from 1992 to 2018 (Fig. S6, Table S1).

We then overlaid the BBS routes over each coarsened raster or county shapefile (for pesticides) and calculated the mean value of all pixels overlapping each route. We plotted all bivariate relationships between the environmental variables and ΔN, Δg, and Δr (both raw and smoothened) across the 1,033 BBS routes, together with their Spearman correlations (Fig. S4).

To link the environmental variables to ΔN, Δg, and Δr we performed Random Forest (*68*), Boosted Regression Trees (*69*), and Extreme Gradient Boosting (*70*), using the *ranger* package (*71*), *gbm* package (*72*), and *xgboost* package (*73*). We used repeated k-folds cross-validation (3 repetitions of 10 folds cross-validation) to select the best performing algorithm of these three. In all algorithms, the response variable was either the raw or spatially smoothed ΔN, Δg, or Δr per route. Hyperparameters were selected following best practices (e.g. $\frac{1}{3}$ of predictors for each split in the Random Forest, very low learning rate for XGBoost for more robust model, etc.). As predictors we used the variables from Table S1.

We dealt with variable collinearity in the following way: if there were two or more predictors with Spearman correlation exceeding 0.5 (Fig. S4), we only chose one of them for the random forest analyses, ending up with 12 predictors. If a variable was found to be important in the selected tree-based algorithm, we interpreted its effect as also potentially attributable to the other discarded variables that were correlated with the important variable. We evaluated variable importance by computing the mean decrease in accuracy while permuting the out-of-bag (OOB) data for each tree in the forest. The most important variable was given an importance of 100, and the other variables were given a percentage of that maximum value. Then, for each variable k, we computed a relative contribution to the explained variance (R^2) of the cross-validation test sets as follows:

$$\text{Importance}_k \text{ to } R^2 = \text{Importance}_k \times \frac{R^2}{\sum \text{Importance}} \quad \text{eq. S24}$$

The resulting variable importance rankings and their respective partial dependence plots are in Figs. 3, S7, S8 and S10.

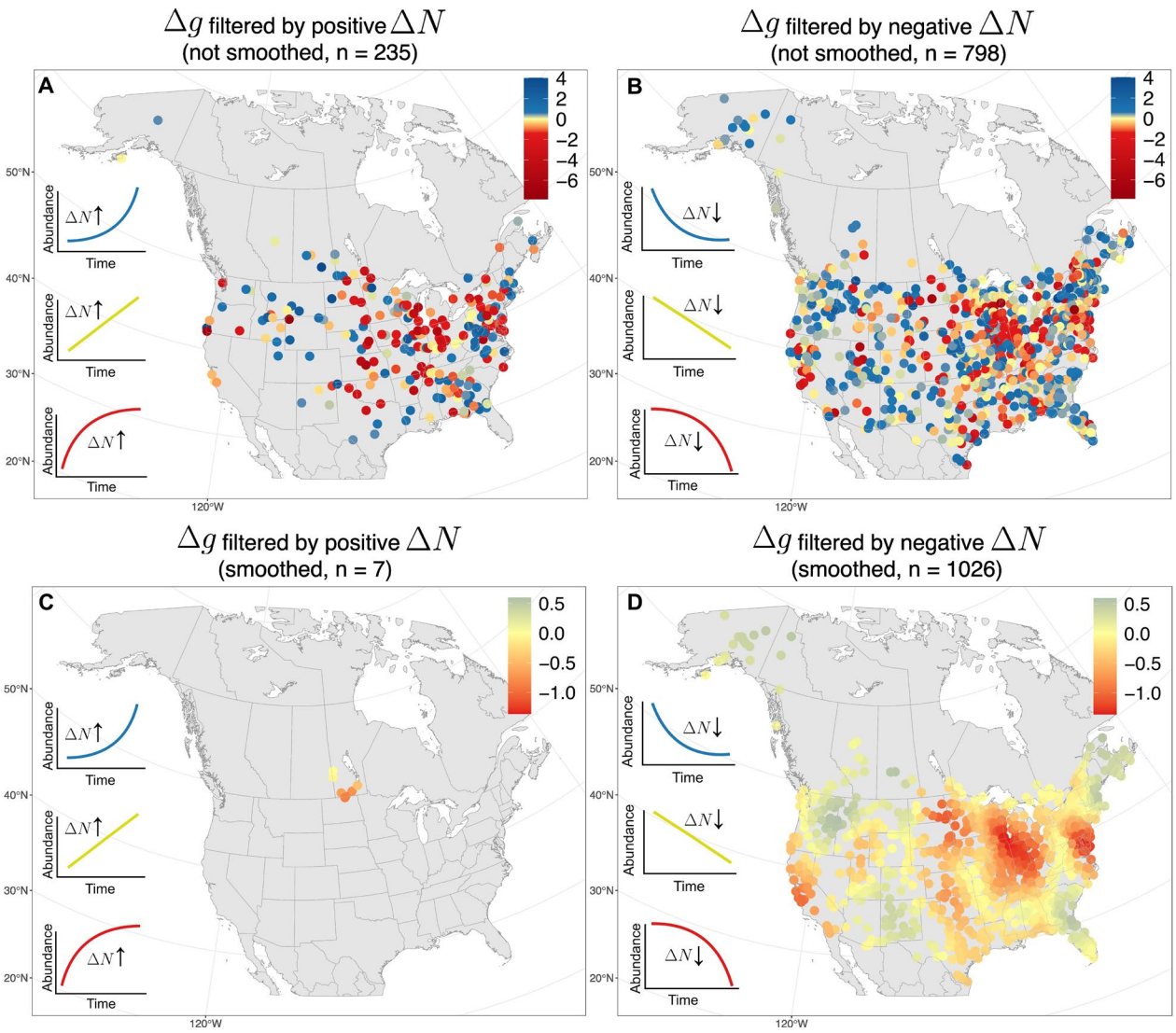

Fig. S1 | Values of growth rate change (Δg) filtered by positive abundance change ΔN (A and C) or negative ΔN (B and D) for the raw output of the models (A and B), and the spatially smoothed values (C and D). In essence, the left column (A and C) shows maps of the accelerated and decelerated abundance increase, while the right column (B and D) shows the acceleration and deceleration of the decline. Inset plots show the shape of ΔN according to the values of Δg. The information on these maps has been summarized in Fig. 2B and D by adding the black dotted circles to indicate regions with positive ΔN.

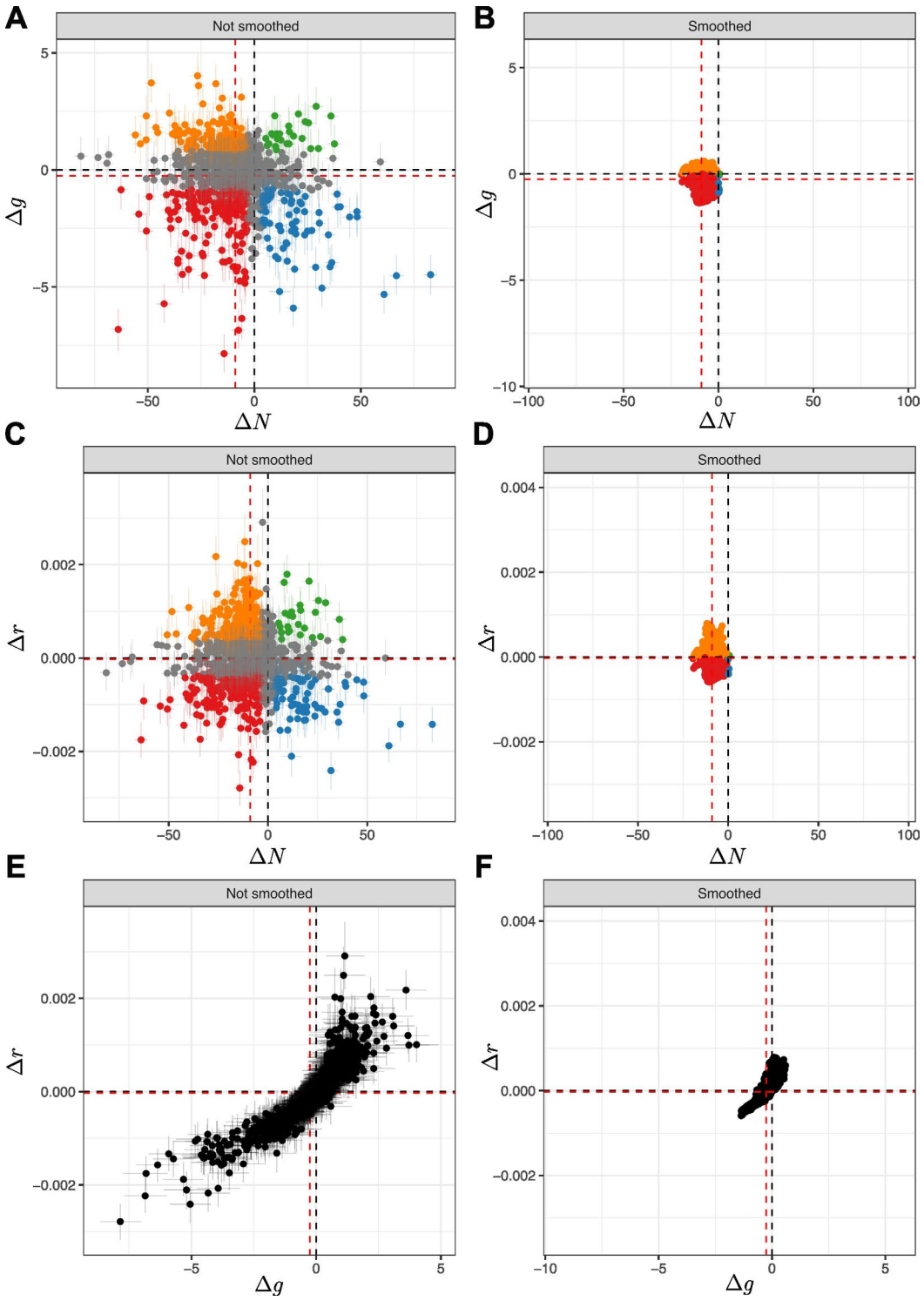

Fig. S2 | Per route values of (A and B) change in abundance (ΔN) vs. change in growth rate (Δg), (C and D) change in abundance (ΔN) vs. change in per capita growth rate (Δg), and (E and F) change in growth rate (Δg) vs. change in per capita growth rate (Δr). Left column (A, C, and E) are the outputs of the model, and right column (B, D, and F) are the spatially smoothed data. Error bars in (A, C, and E) show the 95% Credible Interval of the MCMC propagated uncertainty. Red dotted lines show the average values of ΔN, Δg, or Δr. See Fig. 1 for color scheme details.

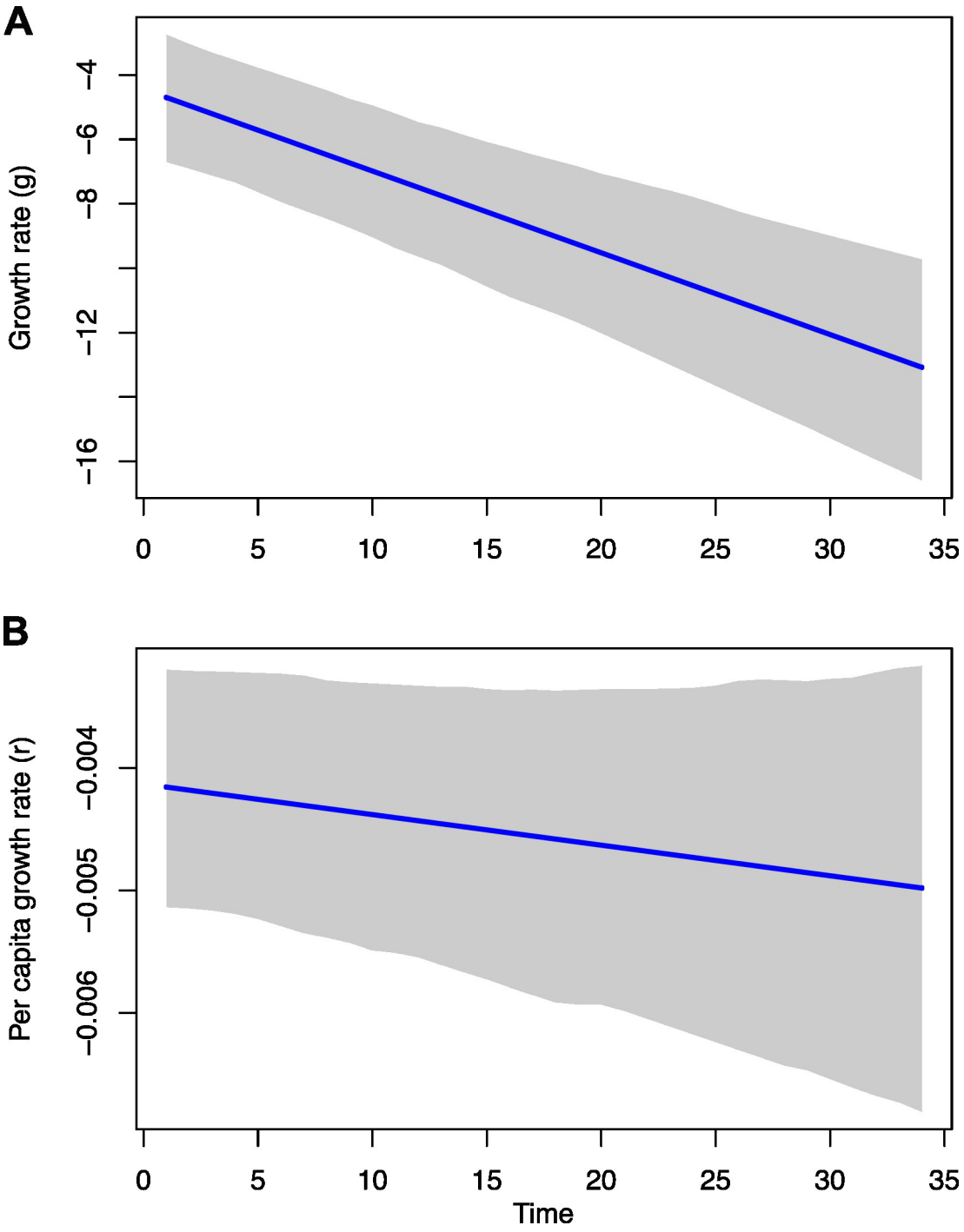

Fig. S3 | Average temporal change in (A) growth rate g, and (B) per capita growth rate r, at the route level (blue line) with 95% credible interval (grey polygons) based on the parameters inferred from the spatial mixed models (eqs. S15 and S16).

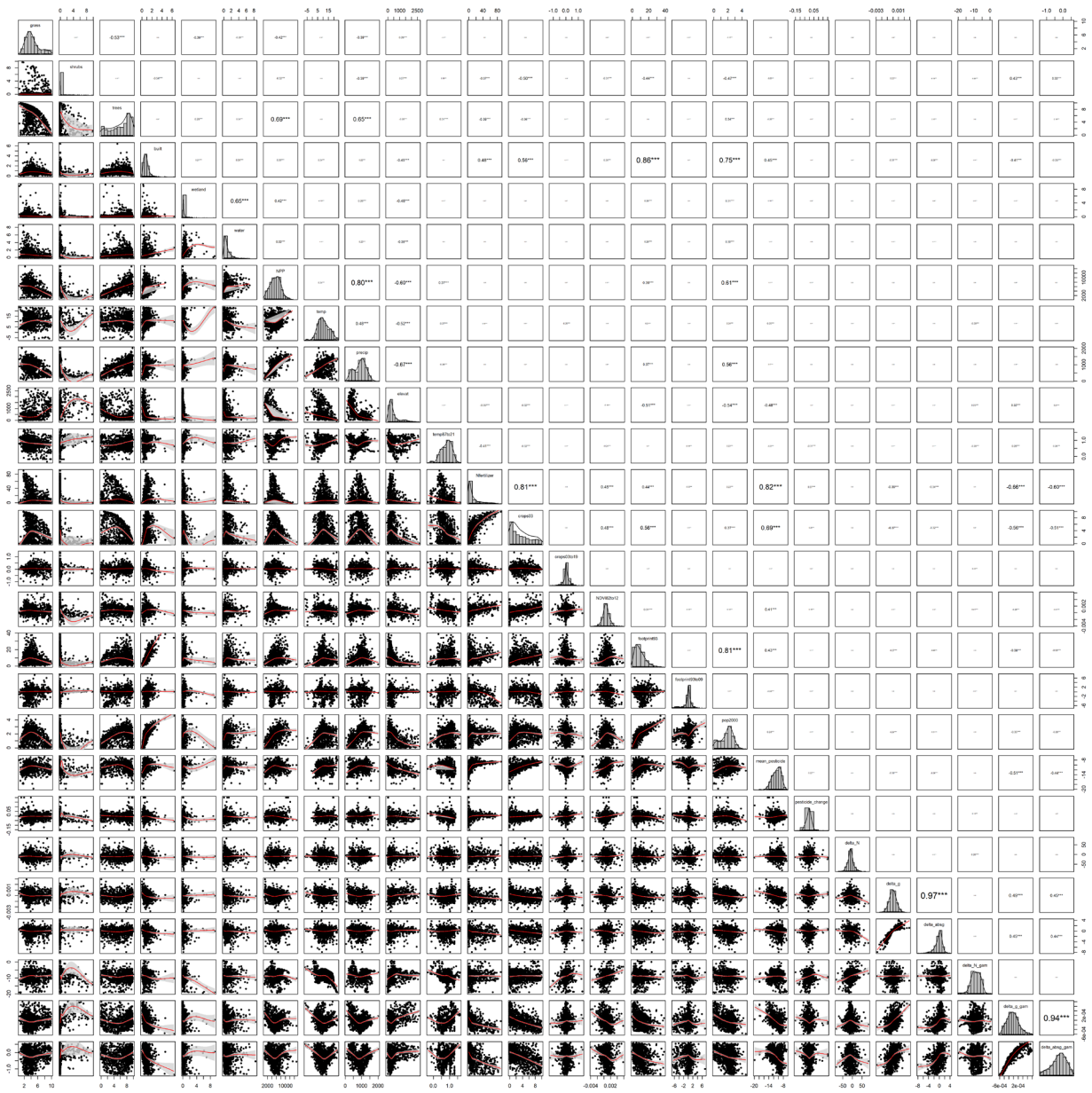

Fig. S4 | Correlations between the environmental and human-related variables, and ΔN, Δg, Δr (raw outputs and spatially smoothed with a GAM). Numbers in the upper right triangle are Spearman correlation coefficients, with larger values in larger letters. For explanation of variable names and details see Table S1.

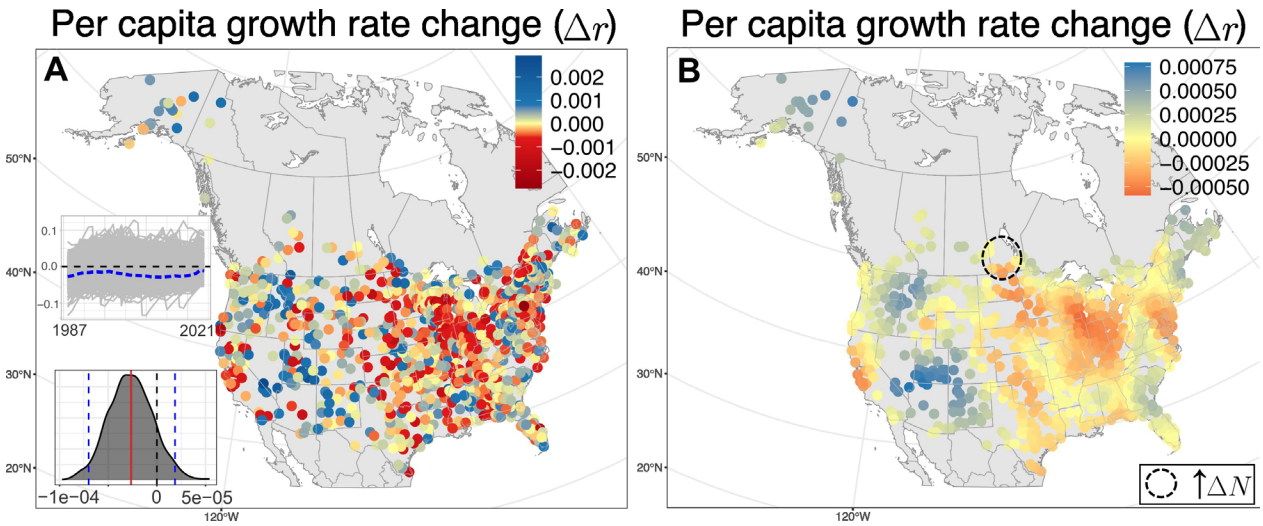

Fig. S5 | Temporal change of per capita growth rate (Δr) for (A) raw outputs and (B) spatially smoothed. Both panels share the same fixed color scale. Dashed circles in (B) mark the only region with positive values of the smoothed ΔN. Inset plots in bottom left show the raw (i.e. not spatially smoothed) trends in per capita growth rates; y-axes in (A) have been signed square root transformed, with the average trend in blue dashed line. The histograms show the posterior distributions of the average slope; red vertical lines are means and dashed blue lines are 95% credible intervals.

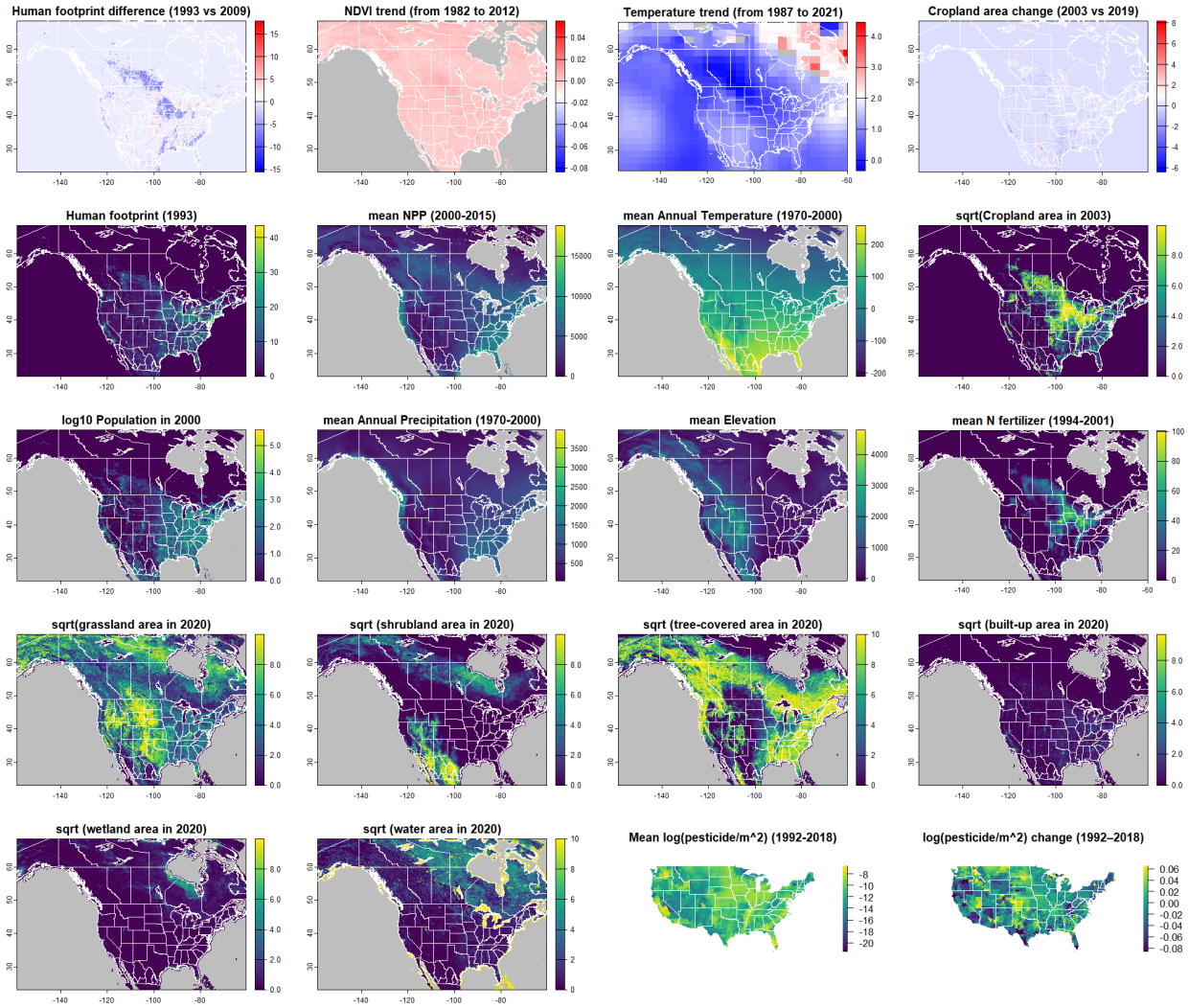

255 **Fig. S6 |** Maps of environmental and human-related variables used in the post-hoc analysis. Details on each are in Table S1.

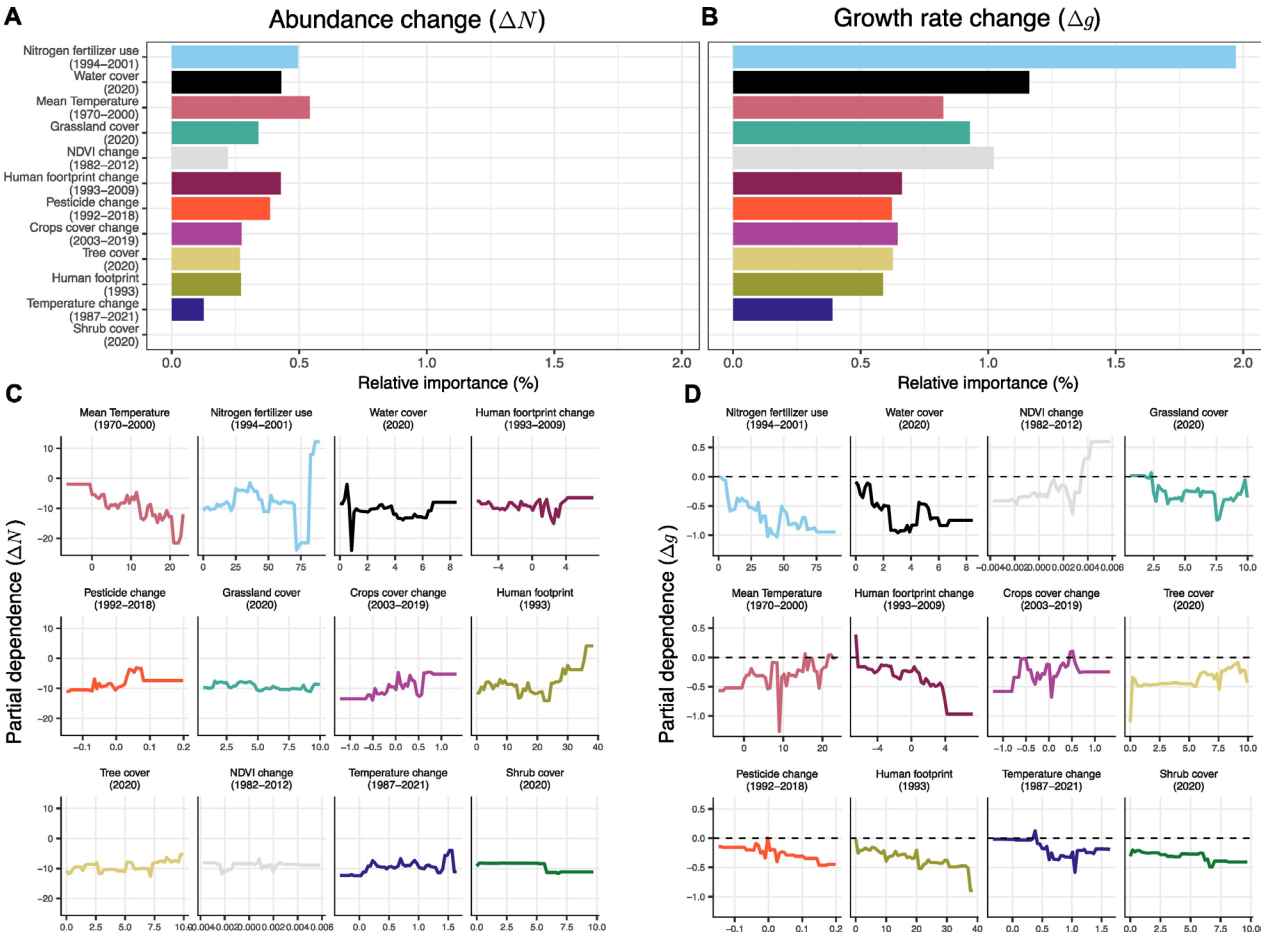

Fig. S7 | Variable importance scores (A and B) and partial dependence plots (C and D) from best performing tree-based models explaining changes in non-smoothed abundance ΔN and growth rate Δg. (A and B). Variable importance scores scaled to R^2 from XGBoost for ΔN (total var. explained $R^2 = 2.6\%$), and for Δg (total var. explained $R^2 = 9.0\%$). (C and D) Partial dependence plots ordered from most to least important, for ΔN and Δg, respectively. Note here that more negative values of Δg indicate accelerated declines in abundance. Predictor variable details are provided in Table S1. To avoid multicollinearity, only a subset of the variables listed in Table S1 was used in the final models (see Methods for details). Importantly, the main explaining variable for both ΔN and Δg are the same as for the smoothed values (Fig.3).

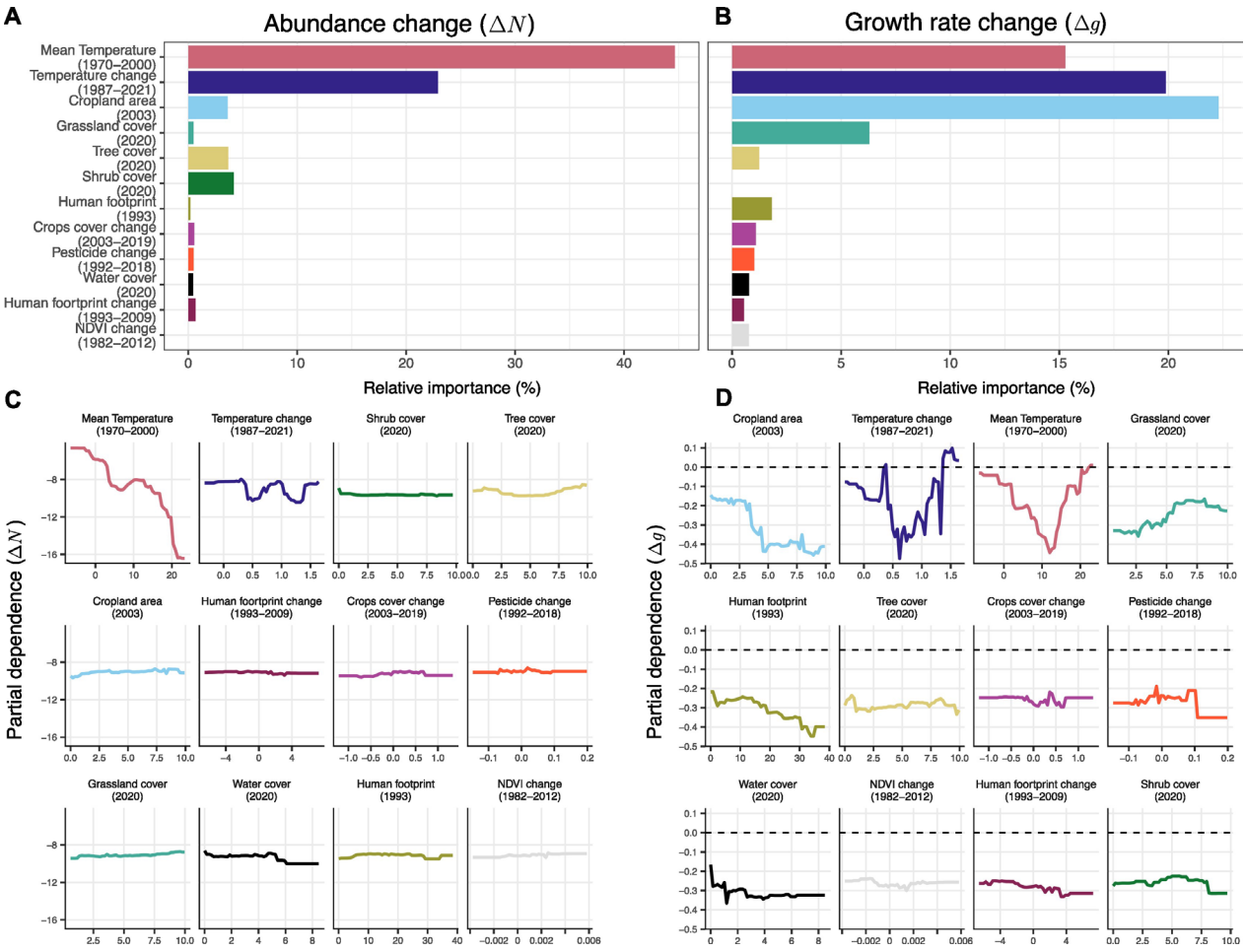

Fig. S8 | Variable importance scores (A and B) and partial dependence plots (C and D) explaining changes in smoothed ΔN and Δg, where the "fertilizer use" covariate has been replaced by "cropland area (2003)". (A and B) Variable importance scores scaled to R^2 from XGBoost for ΔN (total var. explained $R^2 = 83\%$), and for Δg (total var. explained $R^2 = 73\%$). (C and D) Partial dependence plots ordered from most to least important, for ΔN and Δg, respectively. Note here that more negative values of Δg indicate accelerated declines in abundance. The results are consistent with the models with "fertilizer use", corroborating that agriculture is a major driver of accelerating decline of bird abundance.

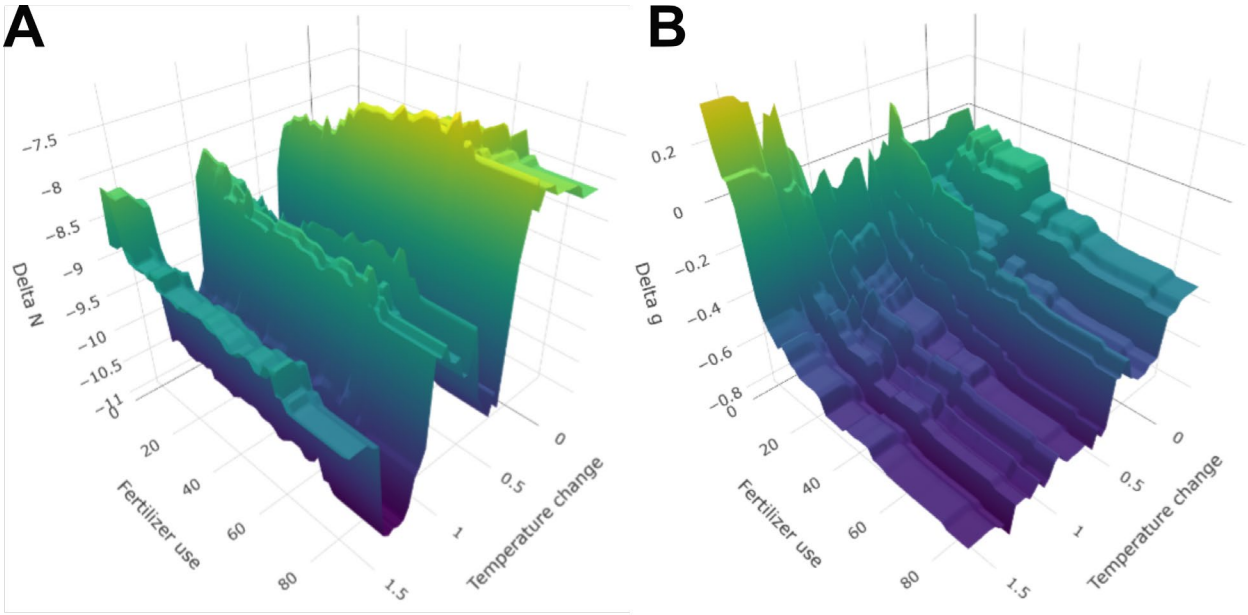

Fig. S9 | Partial dependence plots showing the interaction of both fertilizer use and temperature change on (A) ΔN and (B) Δg.

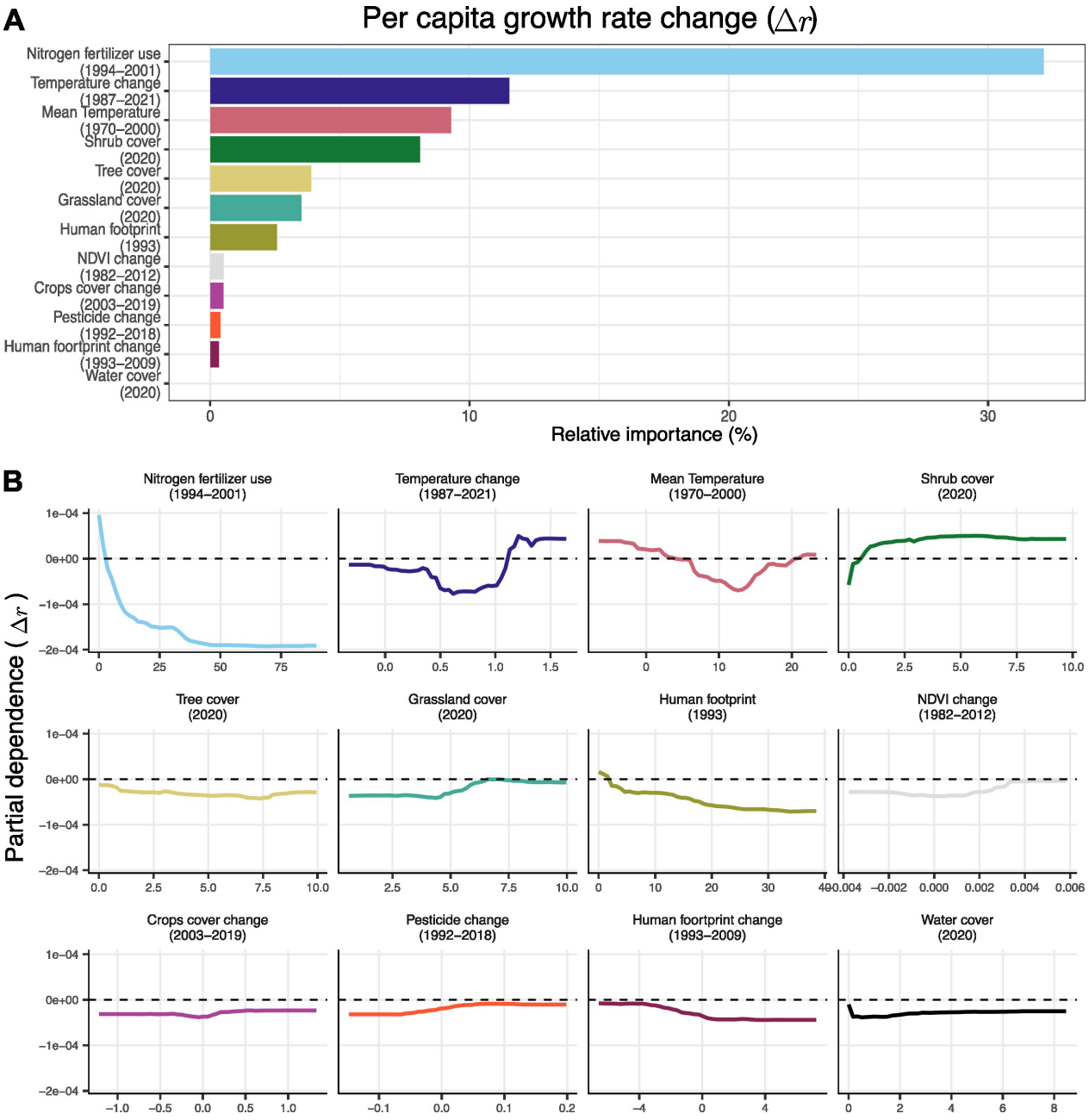

290

Fig. S10 | Variable importance scores (A) and partial dependence plots (B) explaining smoothed changes in per capita growth rate Δr. (A) Variable importance scores scaled to R^2 from Random Forest (total var. explained R^2 = 73%) for Δr. (B) Partial dependence plots ordered from most to least important for Δr.

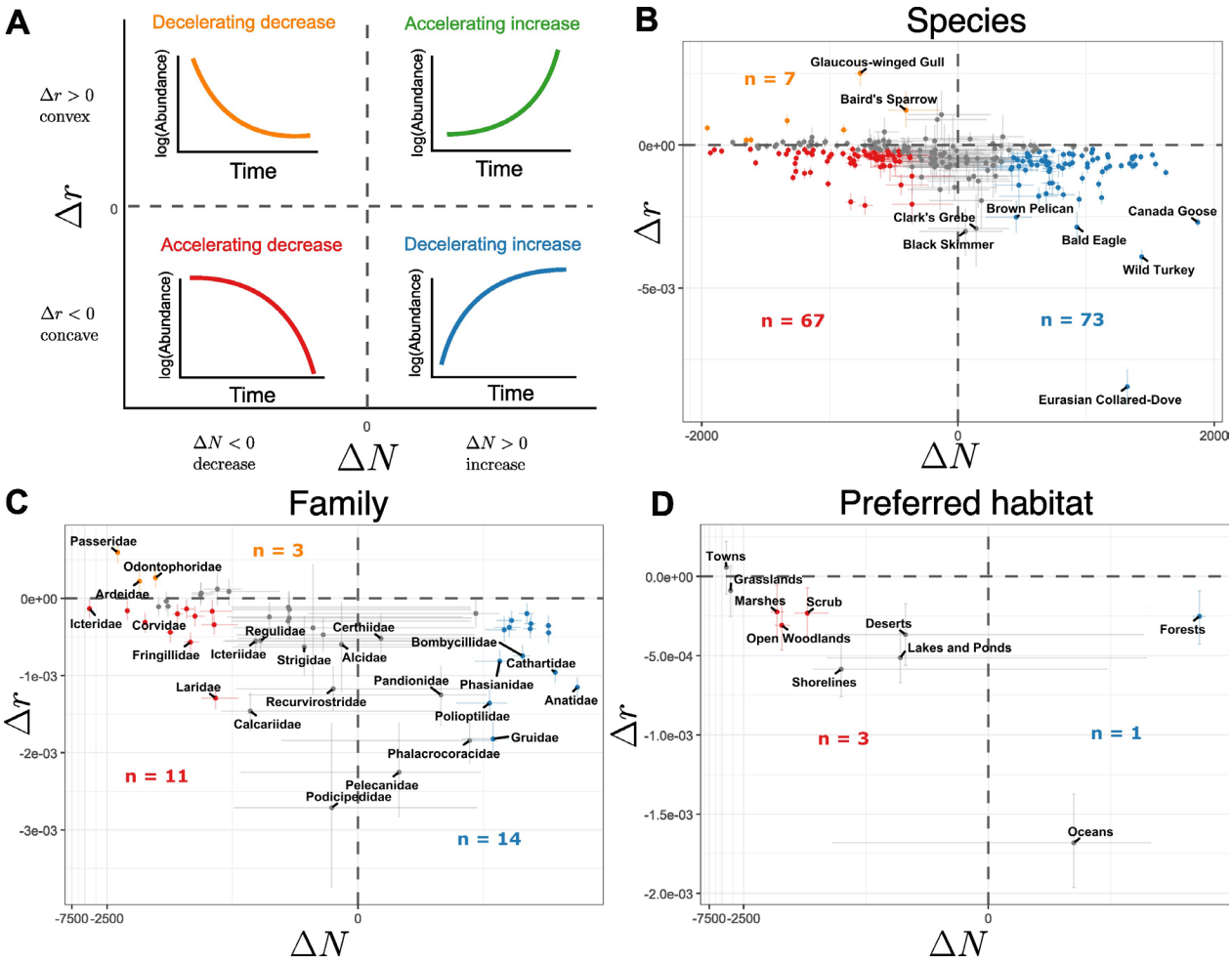

Fig. S11 | Acceleration and deceleration of per-capita growth rate, aggregated across species, families, and habitats. (A) Here, ΔN denotes abundance change, and Δr denotes change in yearly per capita growth rate. Importantly, Δr represents the acceleration or deceleration of changes in log abundance. Zero Δr is either exponential growth (when $\Delta N > 0$) or exponential decay (when $\Delta N < 0$), i.e. constant per-capita growth rate over time. Thus, a population with accelerating increase of abundance ($\Delta g > 0$) can still have constant per-capita growth rate ($\Delta r = 0$). Each point represents ΔN and Δr calculated by aggregating all individuals at the level of (B) a species, (C) a family, and (D) a habitat. Error bars show the 95% credible intervals (CI), and grey points indicate non-significant acceleration or deceleration (i.e. 95% CI overlaps 0 on either axis).

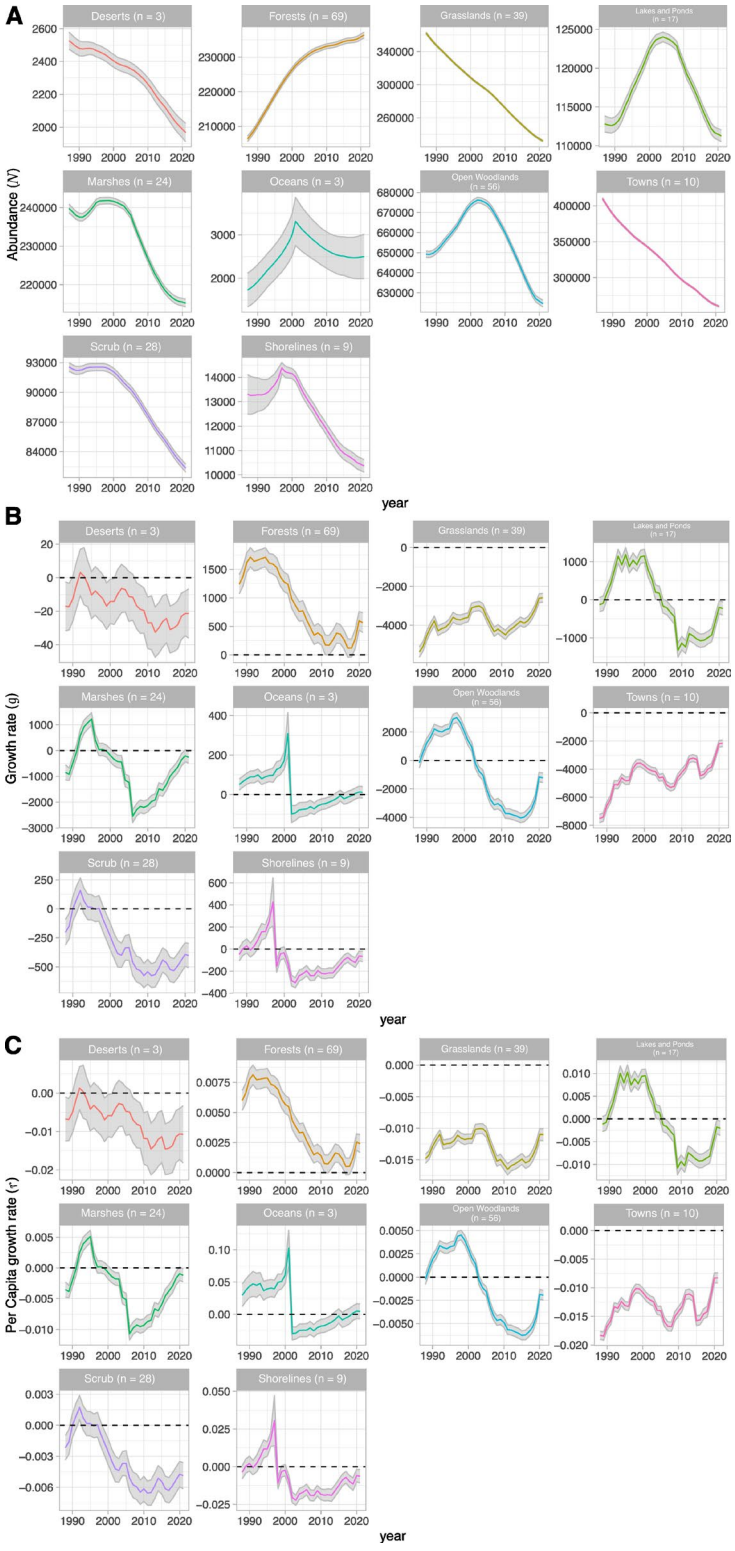

Fig. S12 | Temporal changes in (A) abundance N, (B) yearly growth rate g, and (C) yearly per capita growth rate r for different habitat types. The grey areas show the propagated 95% credible interval of the MCMC chains. The number of species (n) in each habitat is noted.

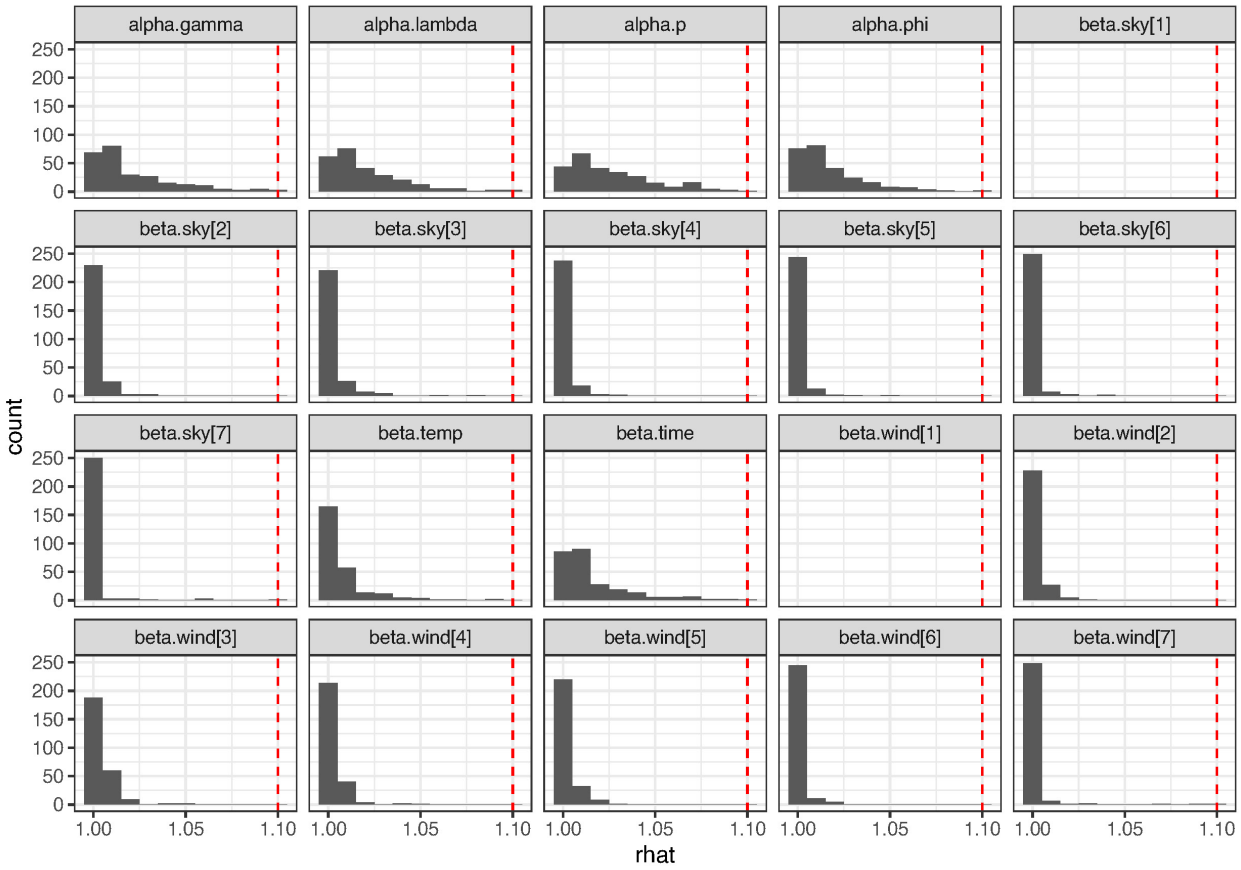

Fig. S13 | Convergence diagnostics of the dynamic N-mixture model. Panels show distributions of the $\hat{R}$ values (i.e. potential scale reduction) for the 261 selected species for each of the 8 parameters included in the dynamic *N*-mixture models. The parameters are: gamma = recruitment, lambda = abundance at time 1, p = detection probability, phi = survival probability, sky = sky condition during the survey, temp = temperature during the survey, time = time of the day of the survey, wind = wind condition during the survey. The 261 species were selected as all parameters $\hat{R} \leq 1.1$.

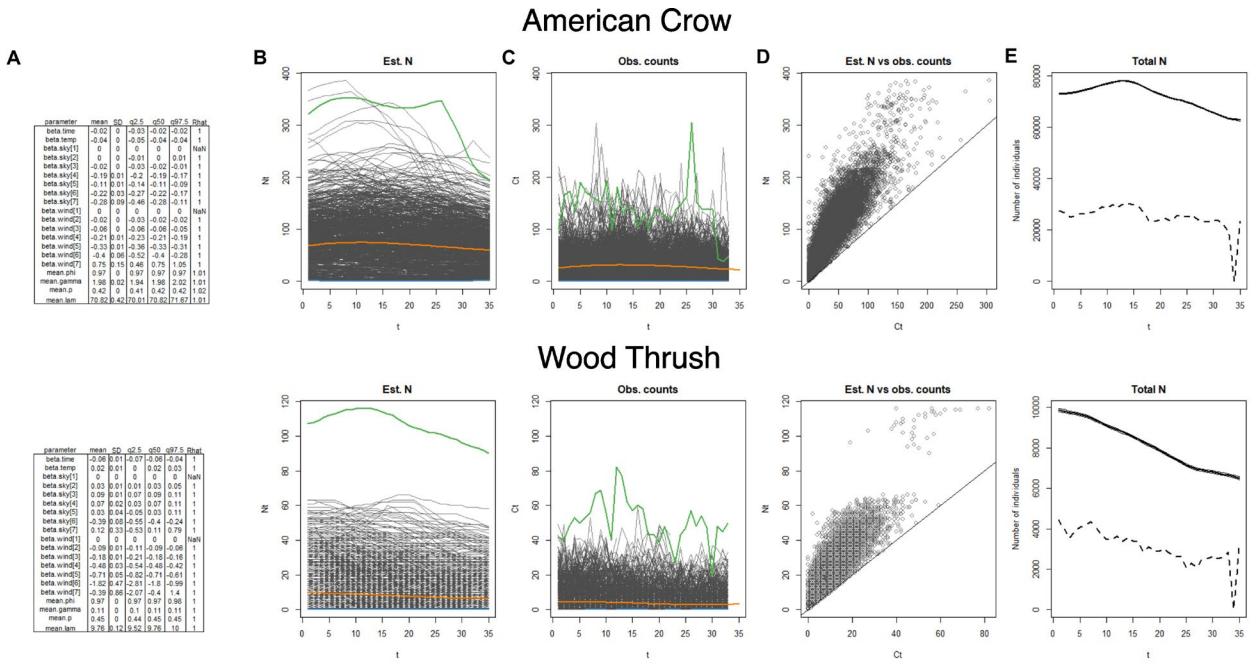

Fig. S14 | Summary of the per species model for 2 selected example species: American Crow (top row) and Wood Thrush (bottom row). (A) Posterior distribution summary of the DM model's parameters. (B) Predicted abundance and (C) observed abundance time series. The green time series is the one with the highest average estimated N, blue line is the time series with the lowest average abundance, orange line is a third-degree polynomial fitted through all of the time series in the plot. (D) Observed vs. predicted abundance. (E) Total (i.e. summed over all BBS routes) predicted abundance (solid line) and total observed abundance (dashed line). These plots for all the original 564 species are available in the linked repository at https://zenodo.org/doi/10.5281/zenodo.18085017).

Table S1 | Details of variables used in the post-hoc correlative analysis of patterns of change and acceleration. We downloaded each variable as a spatial raster in its *original resolution* and aggregated it to the *coarsened resolution*. The aggregation function was either sum (for areas of land cover classes and cropland area) or mean (for the rest of variables). When the original and analyzed resolution are identical in the table, no aggregation was done. We then overlaid each BBS route over the coarsened raster, and we calculated the mean value of all pixels overlapping the route.

Abbreviation	Variable	Unit of the coarsened variable, as used in the analysis	Coarsened resolution (original resolution in brackets), which is the length of pixel side	Function used to coarsen (aggregate) the original raster resolution	Ref.	Available from
grass, shrubs, trees, built, wetland, water	Area of land cover classes (in 2020), square root transformed	Sqrt (% of the class area in a 5 min square)	5 min (30 sec)	sum	(*74*)	"geodata" package in R
NPP	Mean MODIS-derived Net Primary Productivity (MOD17A3 product, 2000-2015)	(kg of carbon per m^2 per year) * 10000	5 km (500 m)	mean	(*75*)	https://lpdaac.usgs.gov/products/mod17a3hgfv061/ (downloaded by Petr Keil in 2019)
temp	Mean annual temperature (1970-2000)	°C	5 min (30 sec)	mean	(*76*)	www.worldclim.org
precip	Mean annual precipitation (1970-2000)	mm	5 min (30 sec)	mean	(*76*)	www.worldclim.org
elevat	Mean elevation above sea level	m	5 min (30 sec)	mean	(*77*)	"geodata" package in R or https://srtm.csi.cgiar.org
temp87to21	Trend of mean annual temperature between 1987 and 2021 (GHCNv4 dataset, smoothing radius 250 km), from local linear regression	Difference in °C between 1987 and 2021	2° (2°)	NA	(*78*, *79*)	https://data.giss.nasa.gov/gistemp/maps/
Nfertilizer	Nitrogen fertilizer use (1994-2001)	kg/ha	0.5° (0.5°)	NA	(*80*)	https://search.earthdata.nasa.gov/, collection "Global Fertilizer and Manure, Version 1: Nitrogen Fertilizer Application"
crops03	Cropland area in 2003, square root transformed	sqrt(% of croplands in the 5 min square)	5 min (30 sec)	sum	(*34*)	"geodata" package in R or https://glad.umd.edu/dataset/croplands
crops03to19	Difference of square root of cropland area between 2003 and 2019	difference in sqrt(% of croplands in the 5 min square)	5 min (30 sec)	calculated from already coarsened rasters	(*34*)	"geodata" package in R or https://glad.umd.edu/dataset/croplands

NDVI82to12	Trend in growing season normalized difference vegetation index (NDVI) between 1982 and 2012	Slope of NDVI vs year regression (Theil-Sen method)	0.08° (0.08°)	NA	(*81*)	https://search.earthdata.nasa.gov, collection "Long-Term Arctic Growing Season NDVI Trends from GIMMS 3g, 1982-2012"
footprint93	Human footprint index in 1993 (HFI_{1993})	Combined index on a scale between 0 (low human pressure) and 50 (high human pressure)	5 min (30 sec)	mean	(*82*)	"geodata" package in R or https://datadryad.org/stash/dataset/doi:10.5061/dryad.052q5
footprint93to09	Difference of human footprint index between 1993 and 2009, HFI_{2009}-HFI_{1993}	Difference between two values of the footprint index (see above)	5 min (30 sec)	calculated from already coarsened rasters	(*82*)	"geodata" package in R or https://datadryad.org/stash/dataset/doi:10.5061/dryad.052q5
pop2000	Human population density in 2000, $\log_{10}(x+1)$ transformed	$\log_{10}$(number of individuals+1)	2.5 min (2.5 min)	NA	(*83*)	https://cmr.earthdata.nasa.gov/search/concepts/C1597158029-SEDAC.html
mean_pesticide	Total amount of 182 pesticide compounds per square meter (eq. S23), averaged over the years between 1992 and 2018	log(kg of pesticide/ county m^2)	County area (county area)	NA	(*65*, *66*)	https://water.usgs.gov/nawqa/pnsp/usage/maps/index.php
pesticide_change	Trend of pesticide use from a linear regression of pesticide use by year, between 1992 and 2018	Slope of mean_pesticide vs year regression	County area (county area)	NA	(*65*, *66*)	https://water.usgs.gov/nawqa/pnsp/usage/maps/index.php